2017

AERODYNAMICS AND ECOMORPHOLOGY OF FLEXIBLE FEATHERS AND MORPHING BIRD WINGS

Brett Klassen Van Oorschot

AERODYNAMICS AND ECOMORPHOLOGY OF FLEXIBLE FEATHERS AND MORPHING BIRD WINGS

By

BRETT KLAASSEN VAN OORSCHOT

Bachelor of Arts in Organismal Biology and Ecology, University of Montana, Missoula, MT, 2011

Dissertation

Presented in partial fulfillment of the requirements
for the degree of

Doctor in Philosophy
in Organismal Biology, Ecology, and Evolution

The University of Montana
Missoula, MT

May 2017

Approved by:

Scott Whittenburg, Dean of The Graduate School
Graduate School

Bret W. Tobalske, Chair
Division of Biological Sciences

Art Woods
Division of Biological Sciences

Zac Cheviron
Division of Biological Sciences

Stacey Combes
College of Biological Sciences, University of California, Davis

Bo Cheng
Mechanical Engineering, Pennsylvania State University

Klaassen van Oorschot, Brett, Ph.D., May 2017

Major: Organismal Biology, Ecology, and Evolution

Aerodynamics and ecomorphology of flexible feathers and morphing bird wings

Chairperson: Bret W. Tobalske

Birds are talented fliers capable of vertical take-off and landing, navigating turbulent air, and flying thousands of miles without rest. How is this possible? What allows birds to exploit the aerial environment with such ease? In part, it may be because bird wings are unlike any engineered wing. They are flexible, strong, lightweight, and dynamically capable of changes in shape on a nearly instantaneous basis (Rayner, 1988; Tobalske, 2007). Moreover, much of this change is passive, modulated only by changes in airflow angle and velocity. Birds actively morph their wings and their feathers morph passively in response to airflow to meet aerodynamic demands. Wings are highly adapted to myriad aeroecological factors and aerodynamic conditions (e.g. Lockwood et al., 1998; Bowlin and Winkler, 2004). This dissertation contains the results of my research on the complexities of morphing avian wings and feathers.

I chose to study three related-but-discrete aspects of the avian wing: 1) the aerodynamics of morphing wings during take-off and gliding flight, 2) the presence and significance of wing tip slots across the avian clade, and 3) the aerodynamic role of the emarginate primary feathers that form these wing tip slots. These experiments ask fundamental questions that have intrigued me since childhood: Why do birds have

different wing shapes? And why do some birds have slotted wing tips? It's fair to say that you will not find definitive answers here—rather, you will find the methodical, incremental addition of new hypotheses and empirical evidence which will serve future researchers in their own pursuits of these questions.

The first chapter explores active wing morphing in two disparate aerodynamic regimes: low-advance ratio flapping (such as during takeoff) and high-advance ratio gliding. This chapter was published in the Journal of Experimental Biology (Klaassen van Oorschot et al., 2016) with the help of an undergraduate researcher, Emily Mistick. We found that wing shape affected performance during flapping but not gliding flight. Extended wings outperformed swept wings by about a third in flapping flight. This finding contrasts previous work that showed wing shape didn't affect performance in flapping flight (Usherwood and Ellington, 2002a, 2002b). This work provided key insights that inspired the second and third chapters of my dissertation.

The second chapter examines the significance of wing tip slots across 135 avian species, ranging from small passerines to large seabirds. This research was completed with the help of an undergraduate international researcher, Ho Kwan Tang, and is currently in press at the Journal of Morphology (Klaassen van Oorschot, in press). These slots are caused by asymmetric emarginations missing from the leading and trailing edge of the primary feathers. We used a novel metric of primary feather emargination that allowed us to show that wing tip slots are nearly ubiquitous across the avian clade. We also showed that emargination is segregated according to habitat and behavioral metrics like flight style. Finally, we showed that emargination scaled with mass. These findings

illustrated that wing tip slots may be an adaptation for efficacy during vertical takeoff rather than efficiency during gliding flight.

In the third chapter, I sought to better understand the function of these slotted primary feathers. In an effort to bridge biology and aeronautics, I collaborated with Richard Choroszucha, an aeronautical engineer from the University of Michigan, on this work. These feathers deflect under aerodynamic load, and it has been hypothesized that they reduce induced drag during gliding flight (Tucker, 1993, 1995). We exposed individual primary feathers to different speeds in the wind tunnel and measured deflection such as bend, twist, and sweep. We found that feather deflection reoriented force, resulting in increased lateral stability and delayed stall characteristics compared to a rigid airfoil. These findings lay the foundation for future biomimetic applications of passive morphing-wing aircraft. I aim to submit this chapter for publication at Bioinspiration & Biomimetics in the summer of 2017.

The following dissertation represents my systematic discovery of avian aerodynamics and follows my progression as a scientist. Combined, the following chapters provide novel insight into the complex nature of morphing avian wings.

REFERENCES

Bowlin MS, Winkler DW. 2004. Natural variation in flight performance is related To timing of breeding in tree swallows (Tachycineta bicolor) in New York. Auk 121:345–353.

Klaassen van Oorschot B, Mistick EA, Tobalske BW. 2016. Aerodynamic consequences of wing morphing during emulated take-off and gliding in birds. J Exp Biol 219:3146–3154.

Klaassen van Oorschot B, Tang HK, Tobalske BW. 2017. Phylogenetics and ecomorphology of emarginate primary feathers. J Morphol in press.

Lockwood R, Swaddle JP, Rayner JMV. 1998. Avian wingtip shape reconsidered: wingtip shape indices and morphological adaptations to migration. J Avian Biol 29:273–292.

Rayner JMV. 1988. Form and Function in Avian Flight. Curr Ornithol 5:1–66.

Tobalske BW. 2007. Biomechanics of bird flight. J Exp Biol 210:3135–3146.

Tucker VA. 1993. Gliding birds: reduction of induced drag by wing tip slots between the primary feathers. J Exp Biol 180:285–310.

Tucker VA. 1995. Drag reduction by wing tip slots in a gliding Harris' hawk, Parabuteo unicinctus. J Exp Biol 198:775–781.

Usherwood JR, Ellington CP. 2002a. The aerodynamics of revolving wings I. Model hawkmoth wings. J Exp Biol 205:1547–1564.

Usherwood JR, Ellington CP. 2002b. The aerodynamics of revolving wings II. Propeller force coefficients from mayfly to quail. J Exp Biol 205:1565–1576.

ACKNOWLEDGEMENTS

It would not have been possible to complete this dissertation without the help, mentorship, and support of my colleagues, committee, friends, and family. Without these people, this journey would have remained a dream.

Above all, I thank my life-partner and co-adventurer, Paige Folsom, for her support and patience throughout this arduous process. She provided the grace and grit that such an endeavor requires when I ran low, and gave me the confidence and support to carry on. I am forever grateful to have her by my side.

I thank my amazing adviser, friend, and mentor, Dr. Bret Tobalske. His thoughtfulness, remarkable scientific mind, indelible curiosity, and daily encouragement kept me on course through trying times. His unmatched expertise and knowledge provided essential insight and presented new challenges that allowed me to grow as a scientist, thinker, and human.

My committee was an incredible source of support. I thank Dr. Art Woods, Dr. Stacey Combes, Dr. Bo Cheng, Dr. Zac Cheviron, Dr. Steve Vogel, and Dr. Dick Hutto for their mentorship, thought-provoking discussion, and personal support. I could not have asked for a better group of scientists to mentor me through this process. Dr. Vogel passed away during the course of my doctoral work, but he remains a source of brilliant and endless inspiration.

I also thank Dr. Ondi Crino. She has been an amazing mentor since before I began my doctoral studies. With her support, I made my first true forays into science, and I am eternally thankful for her friendship and guidance.

I acknowledge with immense gratitude the support of my family: my mother, Lorie; stepfather, Scott; my brother, Kent; and my grandmother, Clara. Their love contributed greatly to my success and well-being throughout my graduate career.

I thank my friends for their constant encouragement: Kileen Marshall, host of the Home for Wayward Boys; Loren and Angela; the Cardy Family; Claudine Tobalske; Rod Collen; Brittany Schroeder; the Tacoma Climbing crew; and my life-long friends in Wilderness & Civilization Program.

I acknowledge individuals who stand out as a life-long source of inspiration and support: Jack Nichols—you're right; Communication is Key. Paul Alaback, thank you for teaching me how more fully appreciate the wildness surrounding us and ask meaningful questions. Carolyn Callaghan, thank you for believing in me when I needed it most. Paul Bailey, your daily jokes kept me sane. And I thank my students, whose questions and curiosity continue to inspire me.

Finally, I thank the American taxpayers for funding my research. This work was made possible with the financial support of the National Science Foundation Graduate Research Fellowship.

TABLE OF CONTENTS **PAGE**

Chapter 1 - Aerodynamic consequences of wing morphing during emulated take-off and gliding in birds 1

Chapter 2 - Phylogenetics and ecomorphology of emarginate primary feathers 35

Chapter 3 - Passive aeroelastic deflection of avian primary feathers 67

AERODYNAMIC CONSEQUENCES OF WING MORPHING DURING EMULATED TAKE-OFF AND GLIDING IN BIRDS

AUTHORS: Brett Klaassen van Oorschot, Emily A. Mistick, Bret W. Tobalske

ABSTRACT

Birds morph their wings during a single wingbeat, across flight speeds, and among flight modes. Such morphing may allow them to maximize aerodynamic performance, but this assumption remains largely untested. We tested the aerodynamic performance of swept and extended wing postures of 13 raptor species in three families (Accipitridae, Falconidae, and Strigidae) using a propeller model to emulate mid-downstroke of flapping during takeoff and a wind tunnel to emulate gliding. Based on previous research, we hypothesized that 1) during flapping, wing posture would not affect maximum ratios of vertical and horizontal force coefficients (C_V:C_H), and that 2) extended wings would have higher maximum C_V:C_H when gliding. Contrary to each hypothesis, during flapping, extended wings had, on average, 31% higher max C_V:C_H ratios and 23% higher C_V than swept wings across all biologically relevant attack angles (α), and, during gliding, max C_V:C_H ratios were similar for both postures. Swept wings had 11% higher C_V than extended wings in gliding flight, suggesting flow conditions around these flexed raptor wings may be different from those in previous studies of swifts (Apodidae). Phylogenetic affiliation was a poor predictor of wing performance, due in part to high intrafamilial variation. Mass was only significantly correlated with extended wing performance during gliding. We conclude wing shape has a greater effect on force per unit wing area during flapping at low advance ratio, such as take-off, than during gliding.

INTRODUCTION

Flying birds use their wings to accomplish a diverse range of behaviors, including takeoff and landing, maneuvering, cruising, and soaring flight. Aerodynamic performance during each type of locomotion may be maximized by altering wing configuration, and birds often dynamically readjust their wing posture as they transition from one behavior to another or as they interact with varying aerodynamic conditions. In particular, birds partially retract their wings into a swept configuration during a variety of aerial behaviors. For example, birds sweep back their wings during upstroke in response to changing flight speeds and modulate wing flexion according to speed and glide angle (Pennycuick, 1968; Tucker, 1987; Tucker and Parrott, 1970). Swifts actively modify wing sweep to alter sink speed and turning rate during maneuvers (Lentink et al., 2007). Eagles sweep their wings back in response to turbulence (Reynolds et al., 2014). Dynamic (i.e. instantaneously variable) wing morphing appears to be ubiquitous among flying birds, and it is generally hypothesized that such morphing optimizes aerodynamic performance.

Although wing morphing is known to alter flight performance during high-speed gliding in ways that influence maneuvering (Lentink et al., 2007), the aerodynamic consequences of wing morphing at different flight speeds and between flapping and gliding is not well-understood. As birds transition from slow to high speed, they continue to flap their wings. During this transition, the body velocity relative to wingtip velocity increases. This relationship is called advance ratio (*J*):

$$J = \frac{V}{\Omega b} \qquad \text{(Eq. 1)}$$

where V = free-stream velocity (m s^{-1}), Ω = angular velocity of the wing (rad s^{-1}), and b = wing length (m). During hovering and very slow flight, such as immediately after takeoff or before landing, J is zero and very low, respectively (Provini et al., 2012; Provini et al., 2014; Tobalske, 2007). J increases with increasing translational velocity of the whole bird, going to infinity during gliding. We tested the effects of swept and extended wing configurations on aerodynamic performance at low and high J.

Current understanding suggests that during flapping flight, subtleties of wing shape have little impact on aerodynamic performance (Usherwood and Ellington, 2002a; Usherwood and Ellington, 2002b). Specifically, propeller models that emulate the mid-downstroke of flapping flight at low-J reveal that aspect ratio (AR, wing span/average wing chord) has virtually no effect on aerodynamic force coefficients except at the highest angles of attack (α) that are probably not biologically relevant for birds (Usherwood and Ellington, 2002a; Usherwood and Ellington, 2002b). For gliding ($J=\infty$), it has long-been assumed that selective pressures have promoted aerodynamic efficiency (i.e. lift:drag ratio) among flying animals (Allen, 1888; Averill, 1927; Beaufrère, 2009; Savile, 1957). The most efficient gliding birds are presumed to be those with either long, high-aspect ratio wings (e.g. frigatebirds and albatrosses) or emarginated, vertically separated primary feathers (e.g. hawks and vultures). These morphologies exhibit extended wings and increase span efficiency by minimizing induced drag caused by the wing-tip vortex (Henningsson et al., 2014; Spedding and McArthur, 2010). In both cases, these efficient wings minimize the effect of the wing-tip vortex by either 1) increasing aspect ratio and thereby reducing the strength of the wingtip vortex(Viieru et al., 2006), or 2) dispersing and shedding the wing-

tip vortex away from the upper surface of the wing in a manner similar to winglets on aircraft (Tucker, 1993; Tucker, 1995).

Cumulatively, these studies led us to form two hypotheses: First, we hypothesized that at low-*J*, both swept and extended wings should produce similar aerodynamic force coefficients (H_1). Second, we hypothesized that at high-*J*, extended wings (due to their increased span and slotted distal primary feathers) should have higher ratios of vertical to horizontal force coefficients (C_V:C_H) compared with swept wings (H_2).

To test these hypotheses, we studied wing performance in 13 raptor species (falcons, hawks, and owls; Falconidae, Accipitridae, and Strigidae) using a propeller model (see Usherwood, 2009; Heers et al., 2011), emulating wing translation during mid-downstroke at low-*J* as in takeoff or landing, and in a wind tunnel, emulating gliding when $J=\infty$. The species in our sample had varying degrees of slotted distal wing planforms when their wings were extended due to emargination of their primary feathers. These birds routinely engage in take-off and landing (low-*J*) and intermittent flight consisting of flapping phases interspersed with glides *(*high-*J).* At low-*J*, birds always flap their wings fully extended. Our study, however, allowed us to explore the aerodynamics associated with swept wings at low-*J*, which could be useful in understanding why birds take off with fully extended wings and also in aiding the design of bird-like micro air vehicles (MAVs). Furthermore, the natural variation in wing shape across the 13 species in this study allowed us to test for aerodynamic differences among clades and explore the evolutionary context of wing morphing.

MATERIALS AND METHODS

Specimens

We measured 26 wings from 13 species of raptors, a large, multiphyletic guild. These birds ranged in mass from 81 g to 1860 g (Table 1). We gathered specimens that had already died from a variety of causes unrelated to this study, and many were missing organs or had become severely dehydrated. For this reason, some masses were estimated using averaged sex-specific values (Dunning Jr., 1992) and are denoted with an asterisk (*) in Table 1.

Wing Preparation

We removed the wings from the bird at the shoulder between the humeral head and the glenoid cavity. We then positioned them in either an extended or swept configuration (Fig. 1), pinned them on a foam board, and dried them at 50° C for 1-3 weeks until the connective tissue hardened. Extended angles were chosen based on the maximum the skeleton and connective tissues would allow, generally forming a straight leading edge. Swept angles were approximated at ~40°, but often changed during drying as the connective tissue contracted. Post-hoc sweep angles were measured between the humeral head, wrist joint, and tip of the leading-edge primary feather, and are reported in Table 1. Once the wings had dried, we drilled into the head of the exposed humerus and inserted a brass tube (4-5 mm dia.) into the hollow bone matrix, cementing it in place using Devcon 5 Minute® epoxy. The brass tubes were counterbalanced internally so we could avoid oscillations associated with spinning unbalanced wings.

Morphometrics, attack angle, and analysis

We measured wing characteristics by photographing and then analyzing them in ImageJ (Schneider et al., 2012). We computed moments of area using a custom MATLAB script (The Mathworks Inc.) (see Table S1). We determined feather emargination based on a prior measure of whole-wing porosity (Heers et al., 2011):

$$Feather\ Emargination = 100\left(\frac{potential\ wing\ area}{actual\ wing\ area}\right) - 100 \quad \text{(Eq. 2)}$$

We used a lateral view of the distal 1/3 of the wing to set geometric angle of attack (α) prior to aerodynamically loading the wings, but considered the attack angle to be zero when lift was zero. Spanwise twist (i.e. washout) was a ubiquitous characteristic among the wings, and the wings deformed under aerodynamic load (Heers et al., 2011) causing the local α to vary greatly. To obtain an objective measure of zero-lift α for comparison among wings, we first interpolated our force values at 1° increments using a cubic spline between empirical measurements for α ranging from -5°<α<+50°. Then we adjusted our measured α to be zero when lift was 0 N.

When possible, we report differences between swept and extended wings using the following percent-change formula, where relevant values (e.g. C_V or F_V) are substituted:

$$Percent\ Change = \frac{(extended\ wing - swept\ wing)}{(extended\ wing)} \times 100 \quad \text{(Eq. 3)}$$

Wind tunnel measurements

To explore the aerodynamics associated with high-*J*, translational flight, we used custom wind tunnels at the Flight Laboratory at the University of Montana (Tobalske et al., 2005) and the Concord Field Station at Harvard University (Tobalske et al., 2003a). We sampled each wing at 8 ms^{-1}. The wing was affixed with a brass rod to a NEMA 23 stepper motor (23W108D-LW8, Anaheim Automation, Inc.) fastened to a force plate (see *Force Measurements* below for details), located outside the tunnels. The wings were rotated through attack angles in 4.5° increments, controlled using an Arcus ACE-SDE controller (Arcus Technology Inc., Livermore, CA, USA). We calculated Reynolds number (*Re*) by measuring the wing chord at the base of the alula feather. To test for effects of aeroelastic deformation at higher velocities, we tested a subset of the wings at 10 ms^{-1} and 14.1ms^{-1} and noted no difference in the vertical or horizontal coefficients. Those results are omitted here for simplicity.

Propeller measurements

We spun the wings like a propeller to emulate mid-downstroke during low-*J* flapping flight (Heers et al., 2011; Usherwood, 2009; Usherwood and Ellington, 2002a; Usherwood and Ellington, 2002b). We applied estimated *in vivo* angular velocities (rad s^{-1}) using known wing-beat frequencies and stroke excursion angles from prior studies (Jackson and Dial, 2011; Tobalske and Dial, 2000). For birds <800g in body mass, we used $\log \Omega = .01966(\log(m)) + 2.0391$ and for birds >800 g, we used $\log \Omega = .3055(\log(m)) + 2.1811$, where Ω is angular velocity and m is mass. The larger birds' wings broke when spun using the angular velocity equation of the smaller birds, necessitating the second equation fitted specifically to birds >800 g. We measured the

vertical force and torque these wings generated using 5°-10° increments in α. We ran several of the wings at various angular velocities and noted no significant difference in the resulting coefficients of aerodynamic force.

For <800 g birds, we used a NEMA 23 stepper motor (23W108D-LW8, Anaheim Automation, Inc.). For >800 g birds, we used NEMA 34 stepper motor (34Y314S-LW8, Anaheim Automation, Inc.) coupled with a 3:1 planetary inline reduction gearbox (GBPH-060x-NP, Anaheim Automation, Inc.). Both motors were controlled using the same Arcus controller used in the wind tunnel measurements.

Force Measurements

We measured aerodynamic forces using a custom force plate (15×15cm platform, 200Hz resonant frequency, Bertec Corporation, Columbus, OH, USA) for wings from birds <800 g, and a Kistler type-9286A force plate (Kistler Instruments Corp., Amherst, NY, USA) for wings from birds >800 g. At each α, we collected data at 1 KHz for several seconds and then filtered those force traces using a 3-Hz low-pass Butterworth filter before taking an average of the forces over the duration of the measurement. Raw force traces contained considerable noise due to aeroelastic flutter (Fig. 2).

For comparisons among wings, we nondimensionalized the forces into vertical and horizontal coefficients using the following equations (see Usherwood and Ellington, 2002a):

Flapping flight:

$$C_V = \frac{2F_V}{\rho\Omega^2 S_2} \qquad C_H = \frac{2Q}{\rho\Omega^2 S_3} \qquad \text{(Eq. 4)}$$

Gliding flight:

$$C_V = \frac{2F_V}{\rho V^2 S} \qquad C_H = \frac{2F_H}{\rho V^2 S} \qquad \text{(Eq. 5)}$$

where C_V is the coefficient of vertical force, C_H is the coefficient of horizontal force, F_V is vertical force (N), F_H is the horizontal force (N), Q is torque (N m) about the z-axis, ρ is air density at Missoula, MT, (978 m elev., 1.07 kg/m^3), or Bedford, MA (41 m elev., 1.204 kg/m^3), Ω is angular velocity of the spinning wing (rad s^{-1}), S is the area (m^2), S_2 is the second moment of area of the wing (m^4), and S_3 is the third moment of area of the wing (m^5, Table S1).

Statistics and phylogenetic analysis

To test for effects of mass on peak C_V:C_H values, we used phylogenetically independent contrasts (PIC; see Felsenstein, 1985) computed using a consensus tree of our experimental species downloaded from birdtree.org (Jetz et al., 2012; Revell, 2012). We tested for effects at the family-level using phylogenetic ANOVAs (R Core Team, 2015; Revell, 2012). We compared continuous variables using phylogenetically independent contrasts within linear models. We used paired T-tests to test for significant differences between swept and extended wings in peak force coefficients and absolute force. We report means ± 1 SD.

RESULTS

Flapping coefficients

For the propeller model (emulating mid-downstroke of flapping at J=0), extended wings had significantly higher peak C_V:C_H than swept wings ($p<.0001$, paired T-test) (Fig. 3). On average, peak C_V:C_H was 3.7±0.8 for extended wings and 2.6±0.9 for swept wings, a 30.9% difference. Changes in C_V were responsible for most differences in C_V:C_H between swept and extended wings (Fig. 4, 5). Swept-wing average peak C_V was 23.1±32.3% lower than extended wings, and average peak C_H was 2.0±59.4% lower. Differences between average swept and extended peak C_V were statistically significant ($p<0.004$) and differences in average peak C_H were nearly significant ($p=0.08$).

The angles at which average peak C_V:C_H occurred were α=17.5°±2.8° for extended wings and α=22.3°±9.2° for swept wings. The highest individual C_V:C_H recorded was 4.8 at α=18° for the extended flapping wing of the rough-legged hawk (*Buteo lagopus*). The red-tailed hawk (*Buteo jamaicensis*) had the highest swept C_V, 1.2, at α=44°, while the rough-legged hawk (*Buteo lagopus*) exhibited the highest extended C_V, 2.0, at α=43° (Table 3, Fig. 6, Table S2).

Gliding coefficients

During modeled gliding flight in the wind tunnel (where $J=\infty$), peak swept and extended wing C_V:C_H ratios were not significantly different ($p=0.5$, paired T-test; Fig. 3 & 4). The average for extended wings was 4.8±1.1 at α=13.1°±2.1°, while the average peak C_V:C_H ratio for swept wings was 4.7±1.6 at α=12.6°±1.9°, a difference of only 0.7%. Similar to flapping, C_V mediated most of the differences in C_V:C_H. In gliding, the swept

wings average peak C_V was 10.6±23.5% higher than extended wings, while average peak C_H was 2.8±14.8% lower (Fig. 4, 5).

The swept wing of the great horned owl (*Bubo virgianus*) had the highest individual peak C_V:C_H, 7.9, at α=11°. The peregrine falcon (*Falco peregrinus*) had the highest swept C_V, 1.4, at α=38°, while the great-horned owl exhibited the highest extended C_V, 1.4, at α=40° (Table 3, Fig. 6, Table S2).

Absolute forces

Absolute forces varied greatly due to differences in wing area (S), shape, and, in the propeller model, angular velocity (Ω), second moment of area (S_2), and third moment of area (S_3). Swept wings had 26.6±10.3% less area, 57.9±14.4% lower S2, and 68.2±14.1% lower S3 than extended wings (Table S1).

During emulated flapping, swept wings produced 68.0±16.1% less peak F_V and 68.9±22.0% less peak F_H than extended wings. The percent change between extended and swept wings for both peak F_V and F_H was not significantly different than the percent change in S_2 or S_3 ($p>0.1$, paired t-test, for both). During emulated gliding, swept wings produced on average 20.6±12.8% less peak vertical force (F_V) and 29.4±11.8% less peak horizontal force (F_H) than extended wings.

The extended wing of the great-horned owl produced the highest vertical force of all the wings tested during emulated gliding flight, 6.7 N (36.7% body weight per wing), at α=39° and 8ms^{-1}. The extended wing of this species produced 3.9 N (21.2% body weight per wing) during emulated flapping flight at α=44° and 15.2 rads^{-1}. During emulated flapping flight, the extended wing of the rough-legged hawk produced the highest vertical

force, 4.4 N (54.0% body weight), at α=43° and 19.6 $rads^{-1}$. The American kestrel (*Falco sparverius*) wing produced the highest force as a percentage of body weight during modeled gliding flight at 66% (132% when considering two wings). The highest force relative to body weight observed on the propeller model came from the wing of the merlin (*Falco columbarius*). It supported 86.8% of body weight (167% for two wings.) On average, individual extended wings produced 47% weight support during emulated gliding flight and 48% weight support during emulated flapping flight. In emulated gliding flight, the average critical attack angle was α=32°±6° for swept wings and α=28°±6° for extended wings, while in emulated flapping flight, the average critical attack angle was α=48°±2° for swept wings and α=45°±4° for extended wings.

Interspecific and morphological patterns

During emulated gliding, accipiter wings had the highest average peak C_V:C_H ratios in both swept and extended configurations (5.3±1.2 and 5.5±0.7, respectively). Conversely, falcons had the lowest average peak C_V:C_H ratios in swept and extended wing configurations during emulated gliding (3.3±0.4 and 3.8±0.8, respectively). Owl wings had average peak C_V:C_H ratios during emulated gliding of 4.9±2.0 for swept wings and 4.4±1.0 for extended wings. During emulated flapping, swept and extended accipiter wings similarly had the highest average peak C_V:C_H ratios (2.9±0.4 and 4.2±0.7, respectively). Falcon (1.8±0.6 and 3.4±0.4, swept and extended) and owl (2.6±1.2 and 3.2±0.7, swept and extended) wings had lower average peak C_V:C_H ratios during emulated flapping. Despite this variation, peak C_V:C_H between families was not significant for any wing posture or flight style (phylogenetic ANOVA, $p>0.4$ for all).

Familial classification was a poor predictor of wing morphological characteristics. Body mass, extended-wing aspect ratio, emargination, area, and wing loading did not vary significantly among families ($p>0.6$ for all, phylogenetic ANOVA). Log-transformed mass, however, was significantly positively correlated with extended average gliding peak $Cv:C_H$ ($p=.02$, $R^2=0.35$, PIC-linear model, Table 2) and nearly significantly positively correlated with swept gliding peak $Cv:C_H$ ($p=.06$, $R^2=0.21$, PIC-linear model). Mass was not positively correlated with swept flapping or extended flapping peak $Cv:C_H$ ($p=0.1$ and .2, $R^2=0.12$ and .07, respectively). Log-transformed extended-wing area was also positively correlated with extended gliding and swept flapping average peak $Cv:C_H$ ($p=0.005$ and 0.036, $R^2=0.49$ and .28, respectively) and also marginally significantly correlated with swept gliding($p=0.061$) and extended flapping ($p=0.07$). No other morphological characteristics significantly correlated with peak $C_V:C_H$ (Table 2). Additionally, mass did not correlate with primary feather emargination ($p=0.3$, phylogenetic ANOVA). Familial means generally exhibited large standard deviations indicating substantial morphological variance among closely-related species.

DISCUSSION

Wing sweep differentially influenced aerodynamic performance on a per-unit-area-basis (i.e. C_V and C_H). During emulated flapping, extended wings outperformed swept wings in both C_V and $C_V:C_H$; whereas during emulated gliding, swept wings outperformed extended wings in C_V and matched performance in $C_V:C_H$. These results provide insight into the relationship between wing posture and aerodynamic performance in raptors.

In emulated flapping flight, angular velocity of the rotating wing causes the wing tips to move more quickly than the wing roots. Since aerodynamic forces vary with the square of local velocity, longer wings produce exponentially greater forces. Furthermore, local flow conditions (as indicated in the coefficients) likely change according to wing posture, and may influence aerodynamic forces. In flapping flight, extended wings had 23.1% higher C_V than swept wings. Thus, in flapping, the 68% increase in peak F_V from swept to extended posture is likely driven by the additive positive effects of S_2 (58% increase) and C_V as wings extend. Extended wings outperform swept wings, even after accounting for S_2, in flapping flight.

During low-*J* flapping flight, the performance of extended wings may benefit from emarginated primary feathers. Previous research has suggested emargination reduces induced drag and increases span efficiency in gliding flight (Spedding and McArthur, 2010; Tucker, 1993; Tucker, 1995). However, our broader comparative sample contrasts with Tucker's findings, because we observed that the effects of tip emargination are likely significant during takeoff (low *J*) but not during gliding (high *J*). This finding may help to explain variation in wing-tip morphology among the diverse array of soaring birds. Raptors must regularly takeoff vertically from the ground and may thus have slotted feathers to increase C_V at low *J*. In contrast, pelagic soarers such as albatross (with pointed wing tips) may rarely experience low-*J* flight due to constant marine surface winds and long, nearly horizontal takeoff trajectories into a prevailing headwind, and indeed avoid flapping flight altogether during windless conditions (Shaffer et al., 2001; Weimerskirch et al., 2000). This could explain the remarkable variation in wing shape between terrestrial and pelagic soaring birds. Future work could explore this hypothesis.

During emulated gliding flight (high-*J*), swept wings had 10.6% higher peak C_V and similar peak Cv:C_H ratios to extended wings. These swept wings had higher vertical force coefficients than extended wings, but due to reduction in S, produced 21% less vertical aerodynamic force. Peak F_V in gliding is thus primarily influenced by the competing effects of reduced S and increased C_V exhibited by swept wings.

In the present study, swept wings during gliding appear to behave like the delta wings of aircraft. Previous work has shown that delta wings can produce lift at post-stall attack angles using vortex lift (Er-El and Yitzhak, 1988; Polhamus, 1966). Vortex lift is caused by flow separation at the leading edge of the wing, and is therefore commonly referred to as a "leading-edge vortex" (LEV). This flow forms a distinct vortex on the top of the wing which runs parallel to the leading edge, increasing lift in a nonlinear fashion. In our experiment, the average critical attack angle (peak C_V) during gliding was $\alpha=32°$ for swept wings and $\alpha=28°$ for extended wings. During flapping, however, both swept and extended wings had high average critical attack angles of $\alpha=48°$ and $\alpha=45°$, respectively. Future research could explore this hypothesis to better understand the aerodynamic mechanism behind increased swept-wing C_V during gliding flight.

Overall, our results were contrary to our two initial hypotheses and surprising for both extremes of advance ratio (*J*). Usherwood and Ellington (2002b) show that the aerodynamics of small- and medium-sized revolving wings (*J*=0; Reynolds numbers [*Re*] = 1100 to 26000) are relatively insensitive to variations in wing morphology and aspect ratio (*AR*). This is the primary evidence that led us to develop our hypothesis (H1). However, close examination of their data indicates our results our consistent for revolving wings at moderate angles of attack ($10°<\alpha<30°$) given that extended wings exhibited higher

AR than swept wings (Table 1). For example, at α=20°, their model hawkmoth wing with *AR*=15.8 generated 43% higher C_V than their model quail wing with *AR*=4.53, while C_H was generally similar for each wing. This implies that the C_V:C_H ratio was also greater for the wing of higher *AR* (Usherwood and Ellington, 2002b, see their Fig. 4C and D) . Their results show that wings with 4.5<*AR*<15.8 produce indistinguishable maximum C_V between 40°<α<60°, whereas the extended raptor wings in our study continued to exhibit higher C_V and C_V:C_H ratios up to α=50° (Figs. 3 & 4). Also, over the relevant range of attack angles, we observed a relatively greater effect for a given *AR* compared to Usherwood and Ellington (2002b). The range of *AR* tested by Usherwood and Ellington (2002b) varied by 3.5x whereas *AR* in our study varied by 1.4x. We thus conclude that extended wings outperform swept wings in emulated flapping flight when *J*=0, but future efforts should seek to test the relative contribution of feather emargination versus *AR*.

The more dramatic differences we report between wing conditions compared with the effects of *AR* upon performance in Usherwood and Ellington (2002b) may be due to a variety of other explanatory variables. Wings in our sample experienced 370,000<*Re*<1,290,000, which is above the critical *Re* of 200,000 where the boundary layer flow transitions from laminar to turbulent (Vogel, 1996). In contrast, Usherwood and Ellington (2002b) tested wings far smaller than those in our experiment, with a maximum *Re* of 26,000. This change in flow regime likely affects force production. In addition to changing *AR* as birds sweep back their wings, camber (cross-sectional profile), washout (spanwise twist), leading-edge angle, and the magnitude of primary feather emargination changes (Tucker, 1987; Withers, 1981). Heers and colleagues (2011) showed that wing porosity (herein called feather emargination) was associated with low lift coefficients and

low lift:drag ratios. In our present study, extended wings exhibited greater feather emargination with less feather overlap than swept wings (Table 1). These changes in morphology could affect local flow conditions and increase span efficiency (Henningsson et al., 2014; Spedding and McArthur, 2010; Tucker, 1987; Tucker, 1993; Tucker, 1995). At low α, average swept wing C_H values were nearly double the extended wing values, further highlighting the potential benefits of emargination at low *J*.

Previous studies of gliding wings ($J=\infty$) show that changes in aspect ratio (*AR*) and sweep can influence aerodynamic forces (Lentink et al., 2007; Pennycuick, 1968; Tucker and Parrott, 1970). Lentink and colleagues (2007) in a study of swift wings (Apodidae) in which feathers do not exhibit significant emargination showed that the lift coefficient was reduced as wings became increasingly swept during gliding. Our results show the opposite trend in raptors. The wings in our sample varied from $1.7<AR<5.0$ and exhibited changes in sweep between 34° and 81° (Table 1), and, although not a statistically significant difference, swept wings had 10.6% higher C_V when $J=\infty$. Additionally, our results indicate almost no difference in peak C_V:C_H between swept and extended wings during emulated gliding flight. A hypothesis for future comparative study is that these differences among species are due to feather emargination.

While coefficients provide insight into the relative levels of force production across species and wing shapes that differ in size, absolute forces, rather than coefficients, are of greater immediate relevance to a bird. Flying at low *J* requires far greater power output than steady translational flight at moderate speeds (Rayner, 1999; Tobalske, 2007; Tobalske et al., 2003b). Slow flight is key to safe transitions between the air and terrestrial perches (Provini et al., 2012; Provini et al., 2014), some forms of prey capture (e.g.

hawking, (Fitzpatrick, 1980; Tobalske, 1996), predator escape (Devereux et al., 2006; van den Hout et al., 2010), and sexually-selected displays. Thus, during these behaviors, birds are likely concerned about maximal force production, rather than efficiency (i.e. C_V:C_H).

Birds generally fully extend their wings during mid-downstroke, and most sweep their wings back during upstroke (Rayner, 1988; Tobalske, 2007). In free-flying thrush nightingales (*Luscinia luscinia*), the upstroke has been shown to become more aerodynamically active as flight speed increases (Spedding et al., 2003) and many species exhibit wing-tip reversal or hand-wing supination in which lift can be produced at very low *J* (Brown, 1963; Crandell and Tobalske, 2011; Crandell and Tobalske, 2015; Tobalske and Dial, 1996), but it is generally thought of as "recovery stroke" between successive downstrokes. It is hypothesized that birds may therefore be sweeping back their wings to reduce drag during the upstroke (Rayner, 1988; Tobalske, 2001). Our results provide additional indirect support for this hypothesis, as swept wings reduced horizontal (i.e. drag) forces 69% during flapping compared to extended wings.

For gliding, our results indicate there is a broad envelope of aerodynamic efficiency available (i.e. C_V:C_H). Since C_V:C_H changes very little as birds sweep their wings, gliding birds are likely able to modulate S without affecting their glide angle by increasing speed during swept-wing flight. This may allow them flexibility when choosing flight speeds to meet environmental demands, such as when gliding between or within thermals. In the present study, wing sweep reduced area 26.6±10.3% on average. Since S and aerodynamic forces scale linearly, it is surprising that F_V does not decrease accordingly with S. As S decreases, F_V decreases by 20.9%. The increase in C_V that occurs with increasing wing sweep during gliding may provide raptors with a subtle mechanism to alter the *magnitude*

of total absolute aerodynamic forces, while modulating angle of attack changes the *relationship* between vertical and horizontal forces.

It is important to note that living birds constantly morph their wings in ways that remain difficult to measure and understanding the precise mechanisms responsible for changes in aerodynamic performance remains challenging. Our propeller and wind tunnel models do not fully represent the complexity of what actually occurs during flapping and gliding flight (Bilo, 1971; Tobalske, 2007).

Conclusions

This experiment shows that wing sweep does not significantly influence C_V:C_H during modeled gliding flight (high *J)* but does have a significant effect on modeled flapping flight such as take-off and landing (low *J)*. Additionally, C_V is higher in swept wings than extended wings during gliding flight, which leads us to speculate that local flow conditions are affected by wing shape. The poor performance of swept wings during spinning offers an explanation for the seemingly universal use of a fully-extended wing posture during downstroke in flapping flight in birds (Tobalske and Dial, 1996; Tobalske et al., 2003a). We hypothesize that relatively low C_V and high C_H values observed for flexed wings during spinning was the result of unfavorable patterns of flow, for example, preventing the formation of a leading-edge vortex (Birch et al., 2004; Ellington et al., 1996; Wang et al., 2004) at low α, and perhaps causing separation of flow (stall) at higher α. In contrast, flexed wings performed better in terms of F_V per unit area in gliding, questioning previous hypotheses regarding the functional significance of emarginated primaries as

adaptations for efficiency during high-*J* flight. Future flow-visualization studies would be useful in testing these ideas.

ACKNOWLEDGEMENTS

We thank Andrew Biewener for use of the wind tunnel and force plate at the Concord Field Station, and Natalie Wright, Ondi Crino, Brandon Jackson, and Pat Little for their help and advice. Two anonymous reviewers provided insightful suggestions that helped us revise the manuscript. Finally, we thank Steven Vogel, who was an extraordinary mentor, a limitless source of brilliant ideas and wit, and remains an inspiration in our hearts and minds.

FUNDING

This research was supported by National Science Foundation grants GRFP DGE−1313190 to BKVO and IOS-0923606, IOS-0919799 and CMMI 1234747 to BWT. Undergraduate research support to EAM was provided by the Herchel-Smith Harvard Research Award.

LIST OF SYMBOLS

J = advance ratio

AR = aspect ratio

α = angle of attack

V = free-stream velocity (m s^{-1}),

Ω = angular velocity of the wing (rad s^{-1})

b = wing length (m).

C_V = coefficient of vertical force

C_H = coefficient of horizontal force

Re = Reynolds number

F_V = vertical force (N)

F_H = horizontal force (N)

Q = torque (N•m) about the z-axis,

ρ = air density

S = wing area (m^2),

S_2 = second moment of area of the wing (m^4)

S_3 = third moment of area of the wing (m^5).

REFERENCES

Allen, J. A. (1888). On the structure of birds in relation to flight, with special reference to recent alleged discoveries in the mechanism of the wing. *Trans. New York Acad. Sci.* 89–100.

Averill, C. K. (1927). Emargination of the long primaries in relation to power of flight and migration. *Condor* 29, 17–18.

Beaufrère, H. (2009). A review of biomechanic and aerodynamic considerations of the avian thoracic limb. *J. Avian Med. Surg.* 23, 173–185.

Bilo, D. (1971). Flugbiophysik von Kleinvögeln. *J. Comp. Physiol. A Neuroethol. Sensory, Neural, Behav. Physiol.* 71, 382–454.

Birch, J. M., Dickson, W. B. and Dickinson, M. H. (2004). Force production and flow structure of the leading edge vortex on flapping wings at high and low Reynolds numbers. *J. Exp. Biol.* 207, 1063–1072.

Brown, R. H. J. (1963). The flight of birds. *Biol. Rev.* 38, 460–489.

Crandell, K. E. and Tobalske, B. W. (2011). Aerodynamics of tip-reversal upstroke in a revolving pigeon wing. *J. Exp. Biol.* 214, 1867–1873.

Crandell, K. E. and Tobalske, B. W. (2015). Kinematics and aerodynamics of avian upstrokes during slow flight. *J. Exp. Biol.* 218, 2518–27.

Devereux, C. L., Whittingham, M. J., Fernández-Juricic, E., Vickery, J. A. and Krebs, J. R. (2006). Predator detection and avoidance by starlings under differing scenarios of predation risk. *Behav. Ecol.* 17, 303–309.

Dunning Jr., J. B. (1992). *CRC Handbook of avian body masses*. CRC Press.

Ellington, C. P., van den Berg, C., Willmott, A. P. and Thomas, A. L. R. (1996). Leading-edge vortices in insect flight. *Nature* 384, 626–630.

Er-El, J. and Yitzhak, Z. (1988). Influence of the aspect ratio on the aerodynamics of the delta wing at high angle of attack. *J. Aircr.* Vol. 25, pp. 200–205.

Felsenstein, J. (1985). Phylogenies and the Comparative Method. *Am. Nat.* 125, 1–15.

Fitzpatrick, J. W. (1980). Foraging behavior of neotropical tyrant flycatchers. *Condor* 82, 43–57.

Hedenström, a, Rosén, M. and Spedding, G. R. (2006). Vortex wakes generated by robins Erithacus rubecula during free flight in a wind tunnel. *J. R. Soc. Interface* 3, 263–276.

Heers, A. M., Tobalske, B. W. and Dial, K. P. (2011). Ontogeny of lift and drag production in ground birds. *J. Exp. Biol.* 214, 717–725.

Henningsson, P., Hedenström, A. and Bomphrey, R. J. (2014). Efficiency of lift production in flapping and gliding flight of swifts. *PLoS One* 9,.

Jackson, B. E. and Dial, K. P. (2011). Scaling of mechanical power output during burst

escape flight in the Corvidae. *J. Exp. Biol.* 214, 452–461.

Jetz, W., Thomas, G. H., Joy, J. B., Hartmann, K. and Mooers, A. O. (2012). The global diversity of birds in space and time. *Nature* 491, 444–448.

Lentink, D., Müller, U. K., Stamhuis, E. J., de Kat, R., van Gestel, W., Veldhuis, L. L. M., Henningsson, P., Hedenström, A., Videler, J. J. and van Leeuwen, J. L. (2007). How swifts control their glide performance with morphing wings. *Nature* 446, 1082–1085.

Pennycuick, C. J. (1968). A wind-tunnel study of gliding flight in the pigeon *Columba livia*. *J. Exp. Biol.* 49, 509–526.

Polhamus, E. C. (1966). A concept of the Vortex Lift of Sharp-Edge Delta Wings Based on a Leading-Edge-Suction Analogy. *Natl. Aeronaut. Sp. Adm.* Nasa Techn,.

Provini, P., Tobalske, B. W., Crandell, K. E. and Abourachid, A. (2012). Transition from leg to wing forces during take-off in birds. *J. Exp. Biol.* 4115–4124.

Provini, P., Tobalske, B. W., Crandell, K. E. and Abourachid, A. (2014). Transition from wing to leg forces during landing in birds. *J. Exp. Biol.* 2659–2666.

R Core Team (2015). R: A language and environment for statistical computing.

Rayner, J. V. (1988). Form and Function in Avian Flight. In *Current Ornithology SE - 1* (ed. Johnston, R.), pp. 1–66. Springer US.

Rayner, J. M. V. (1999). Estimating power curves of flying vertebrates. *J. Exp. Biol.* 202, 3449–3461.

Revell, L. J. (2012). phytools: an R package for phylogenetic comparative biology (and other things). *Methods Ecol. Evol.* 3, 217–223.

Reynolds, K. V., Thomas, A. L. R. and Taylor, G. K. (2014). Wing tucks are a response to atmospheric turbulence in the soaring flight of the steppe eagle *Aquila nipalensis*. *J. R. Soc. Interface* 11, 20140645.

Savile, D. B. O. (1957). Adaptive evolution in the avian wing. *Evolution (N. Y).* 11, 212–224.

Schneider, C. A., Rasband, W. S. and Eliceiri, K. W. (2012). NIH Image to ImageJ: 25 years of image analysis. *Nat. Methods* 9, 671–675.

Shaffer, S. A., Costa, D. P. and Weimerskirch, H. (2001). Behavioural factors affecting foraging effort of brreeding wandering albatrosses. *J. Anim. Ecol.* 70, 864–874.

Spedding, G. R. and McArthur, J. (2010). Span Efficiencies of Wings at Low Reynolds Numbers. *J. Aircr.* 47, 120–128.

Spedding, G. R., Rosén, M. and Hedenström, a (2003). A family of vortex wakes generated by a thrush nightingale in free flight in a wind tunnel over its entire natural range of flight speeds. *J. Exp. Biol.* 206, 2313–2344.

The Mathworks Inc. MATLAB and Statistics Toolbox Release.

Tobalske, B. W. (1996). Scaling of muscle composition, wing morphology, and

intermittent flight behavior in woodpeckers. *Auk* 113, 151–177.

Tobalske, B. W. (2001). Morphology, Velocity, and Intermittent Flight in Birds. *Am. Zool.* 41, 177–187.

Tobalske, B. W. (2007). Biomechanics of bird flight. *J. Exp. Biol.* 210, 3135–3146.

Tobalske, B. W. and Dial, K. P. (1996). Flight kinematics of black-billed magpies and pigeons over a wide range of speeds. *J. Exp. Biol.* 199, 263–80.

Tobalske, B. W. and Dial, K. P. (2000). Effects of body size on take-off flight performance in the Phasianidae (Aves). *J. Exp. Biol.* 203, 3319–3332.

Tobalske, B. W., Hedrick, T. L. and Biewener, A. A. (2003a). Wing kinematics of avian flight across speeds. *J. Avian Biol.* 34, 177–184.

Tobalske, B. W., Hedrick, T. L., Dial, K. P. and Biewener, A. A. (2003b). Comparative power curves in bird flight. *Nature* 421, 363–6.

Tobalske, B. W., Puccinelli, L. A. and Sheridan, D. C. (2005). Contractile activity of the pectoralis in the zebra finch according to mode and velocity of flap-bounding flight. *J. Exp. Biol.* 208, 2895–2901.

Tucker, V. A. (1987). Gliding birds: the effect of variable wing span. *J. Exp. Biol.* 133, 33–58.

Tucker, V. A. (1993). Gliding birds: reduction of induced drag by wing tip slots between the primary feathers. *J. Exp. Biol.* 180, 285–310.

Tucker, V. A. (1995). Drag reduction by wing tip slots in a gliding Harris' hawk, *Parabuteo unicinctus* . *J. Exp. Biol.* 198, 775–81.

Tucker, V. A. and Parrott, G. C. (1970). Aerodynamics of gliding flight in a falcon and other birds. *J. Exp. Biol.* 52, 345–367.

Usherwood, J. R. (2009). The aerodynamic forces and pressure distribution of a revolving pigeon wing. *Exp. Fluids* 46, 991–1003.

Usherwood, J. R. and Ellington, C. P. (2002a). The aerodynamics of revolving wings I. Model hawkmoth wings. *J. Exp. Biol.* 205, 1547–1564.

Usherwood, J. R. and Ellington, C. P. (2002b). The aerodynamics of revolving wings II. Propeller force coefficients from mayfly to quail. *J. Exp. Biol.* 205, 1565–1576.

van den Hout, P. J., Mathot, K. J., Maas, L. R. M. and Piersma, T. (2010). Predator escape tactics in birds: Linking ecology and aerodynamics. *Behav. Ecol.* 21, 16–25.

Viieru, D., Tang, J., Lian, Y., Liu, H. and Shyy, W. (2006). Flapping and Flexible Wing Aerodynamics of Low Reynolds Number Flight Vehicles. *44th AIAA Aerosp. Sci. Meet. Exhib.* 1–18.

Vogel, S. (1996). *Life in moving fluids: The physical biology of flow*. 2nd ed. Princeton, NJ: Princeton University Press.

Wang, Z. J., Birch, J. M. and Dickinson, M. H. (2004). Unsteady forces and flows in low

Reynolds number hovering flight: two-dimensional computations vs robotic wing experiments. *J. Exp. Biol.* 207, 449–460.

Weimerskirch, H., Guionnet, T., Martin, J., Shaffer, S. a and Costa, D. P. (2000). Fast and fuel efficient? Optimal use of wind by flying albatrosses. *Proc. Biol. Sci.* 267, 1869–1874.

Withers, P. C. (1981). An aerodynamic analysis of bird wings as fixed aerofoils. *J. Exp. Biol.* 90, 143–162.

TABLES

Table 1: Morphological and experimental attributes of specimen wings.

	Species	Common Name	4-Letter Abbr.	Mass (g)	Angular Vel.	Area (m^2)		Length (m)		Aspect Ratio		Sweep Angle		Feather Emargination		Reynolds Number	
					(rad/sec)	Ext	Swept	Ext	Swept	Ext	Swept	Ext	Swept	Ext	Swept	Ext	Swept
Falconidae	Falco sparverius	American kestrel	AMKE	80.8	46.7	0.017	0.011	0.285	0.201	4.7	3.6	176	109	8.08	2.24	370,000	400,000
	Falco columbarius	Merlin	MERL	146.9	40.9	0.031	0.015	0.338	0.158	3.7	1.7	159	78	1.69	0.13	570,000	600,000
	Falco peregrinus	Peregrine falcon	PEFA	762.8	31.9	0.051	0.036	0.487	0.326	4.7	3	131	92	0.47	0.22	770,000	810,000
Accipitridae	Accipiter striatus	Sharp-shinned hawk	SSHA	161.1	40.2	0.019	0.015	0.308	0.219	5	3.1	157	113	2.52	1.56	450,000	450,000
	Circus cyaneus	Northern harrier	NOHA	420*	32.6	0.053	0.037	0.443	0.283	3.7	2.2	136	88	3.75	0.7	800,000	850,000
	Accipiter gentilis	Northern goshawk	NOGO	420*	32.6	0.065	0.054	0.459	0.366	3.2	2.5	147	112	1.79	0.81	960,000	920,000
	Accipiter cooperii	Cooper's hawk	COHA	452.2	32	0.049	0.039	0.432	0.337	3.8	2.9	159	120	3.95	1.56	750,000	780,000
	Buteo lagopus	Rough-legged hawk	RLHA	820	19.6	0.097	0.076	0.635	0.423	4.1	2.4	169	113	2.8	0.33	890,000	1,060,000
	Buteo jamaicensis	Red-tailed hawk	RTHA	1250*	17.2	0.100	0.075	0.666	0.526	4.5	3.7	178	119	3.19	1.19	880,000	1,130,000
Strigidae	Aegolius acadicus	Northern saw-whet owl	NSWO	92.6	45.3	0.013	0.011	0.220	0.170	3.6	2.7	138	104	0.64	0.45	430,000	420,000
	Megascops kennicottii	Western screech-owl	WESO	214.3	37.8	0.026	0.017	0.315	0.203	3.7	2.5	163	101	4.9	0.74	580,000	590,000
	Asio otus	Long-eared owl	LEOW	258.2	36.2	0.046	0.034	0.427	0.322	4	3	147	104	2.82	0.93	680,000	700,000
	Bubo virginianus	Great Horned owl	GHOW	1860	15.2	0.127	0.115	0.670	0.573	3.5	2.9	189	142	1.7	0.3	1,030,000	1,290,000

* masses are estimates from Dunning Jr. (1992).

Table 2: Summary of results of statistical tests (p-values) for significant effects of posture, flight style, and morphology upon aerodynamic performance of wings of 13 species of raptors (phylogenetic ANOVA for all; * indicates p<0.05).

	Extended AR	Emargination	Log(extended area)	Wing loading	Log(mass)
Extended Gliding	0.87	0.69	.005*	0.25	0.02*
Swept Gliding	0.53	0.64	0.061	0.17	0.06
Extended Flapping	0.48	0.59	0.07	0.87	0.19
Swept Flapping	1.00	0.94	.036*	0.69	0.14

Table 3: Peak coefficients of vertical and horizontal force, C_V and C_H, observed during experiments using wings from 13 species of raptors.

	Species	Extended Gliding		Swept Gliding		Gliding C_V:C_H		Extended Flapping		Swept Flapping		Flapping C_V:C_H	
		Peak C_V	Peak C_H	Peak C_V	Peak C_H	Extended	Swept	Peak C_V	Peak C_H	Peak C_V	Peak C_H	Extended	Swept
Falconidae	Falco sparverius	0.88	0.9	1.01	0.87	3.15	3.48	1.2	0.96	0.93	1	3.69	2.64
	Falco columbarius	0.82	0.76	1.08	0.84	3.19	2.8	1.22	0.91	0.94	0.82	2.9	1.41
	Falco peregrinus	1.14	0.94	1.39	0.81	4.95	3.59	1.47	0.91	0.8	0.66	3.6	1.45
Accipitridae	Accipiter striatus	0.95	0.89	1.11	0.78	4.29	6.45	1	0.82	1.1	1.06	3.1	2.26
	Circus cyaneus	0.94	0.69	1.34	0.78	4.96	3.41	1.2	0.66	1.12	0.69	4.56	3.47
	Accipiter gentilis	1.18	0.95	1.16	0.88	6.3	5.09	1.53	0.96	0.87	0.64	4.54	3.23
	Accipiter cooperii	0.94	0.81	1.03	0.8	5.24	4.17	1.21	0.66	0.99	0.71	4.7	2.91
	Buteo lagopus	1.31	0.9	0.94	0.67	5.98	5.94	1.95	1.25	1	0.68	4.75	2.89
	Buteo jamaicensis	1.21	0.98	1.06	0.77	6.24	6.42	1.76	1.45	1.24	1.07	3.49	2.76
Strigidae	Aegolius acadicus	1	0.71	1.01	0.77	3.52	3.24	1.77	1.51	0.9	1.26	2.1	1.47
	Megascops kennicottii	0.84	0.78	1.3	0.83	3.3	3.04	1.47	1.09	0.68	0.5	3.1	1.37
	Asio otus	0.95	0.52	1.06	0.66	5.62	5.33	0.67	0.23	1.14	0.66	3.93	3.17
	Bubo virginianus	1.36	0.82	1.02	0.68	4.95	7.9	1.86	1.29	1.12	0.71	3.68	4.25
	Average	1.04	0.82	1.12	0.78	4.75	4.68	1.41	0.98	0.99	0.80	3.70	2.56
	SD (±)	0.17	0.12	0.14	0.07	1.11	1.56	0.36	0.34	0.15	0.21	0.76	0.88

FIGURES

Figure 1: Swept and Extended wings – Birds are capable of morphing their wings into a swept and extended configuration, resulting in reduced area, increased leading edge angle, and reduction of wing-tip slots. Pictured here are the wings of a sharp-shinned hawk (*Accipiter striatus*).

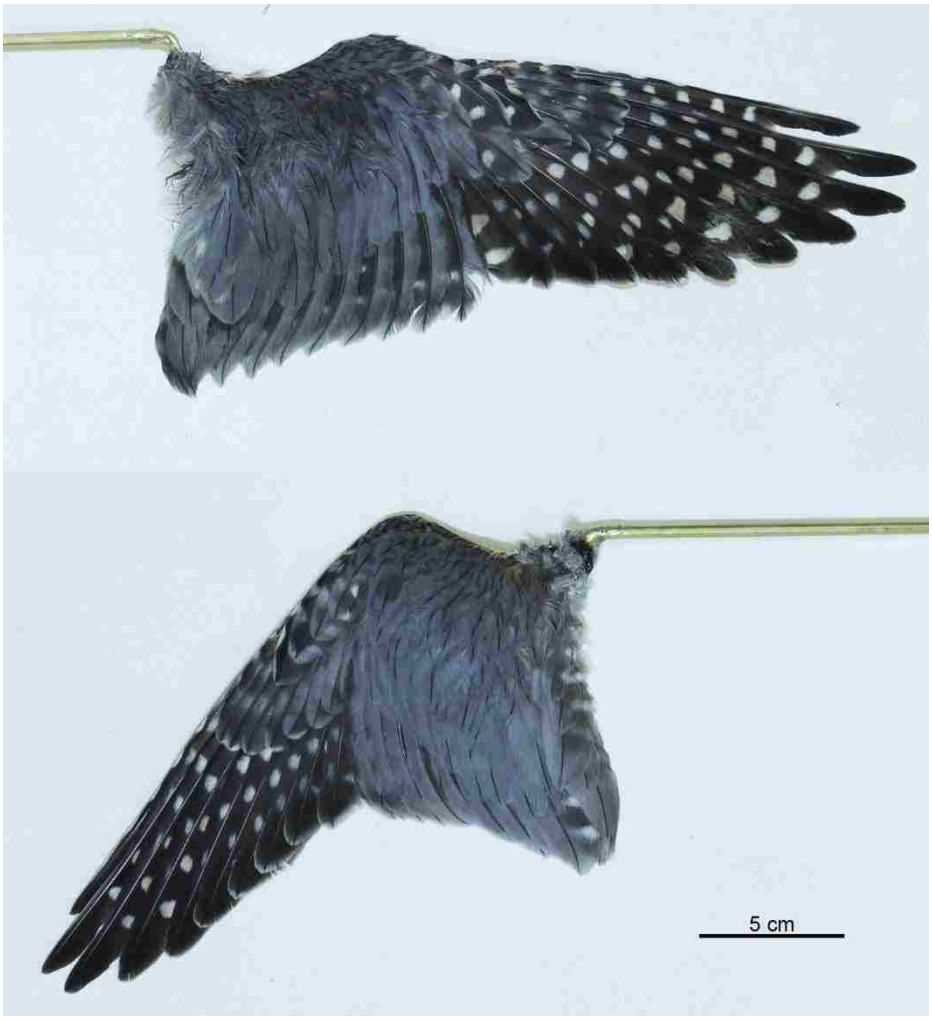

Figure 2: Actual force measures for peregrine falcon (*Falco peregrinus*) extended wing in gliding flight (a) and flapping flight (b). Sample taken at 1000 Hz. Green lines represent data filtered at 3 Hz using a low-pass Butterworth filter.

(a)

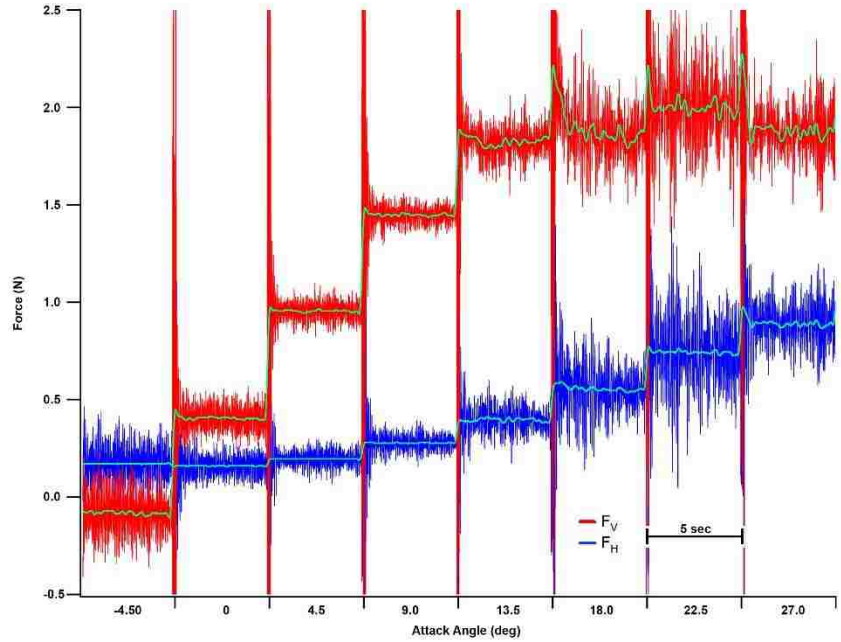

(b)

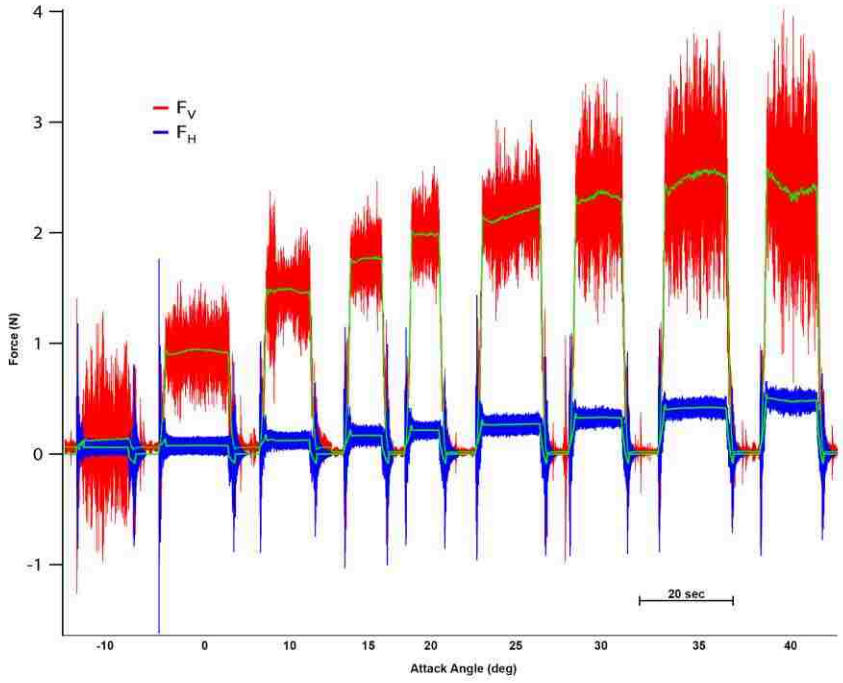

Figure 3: Average ratios of vertical to horizontal force coefficient (C_V:C_H) as a function of angle of attack (α) of the wing for all species (N=13). The shaded regions represent ± SD.

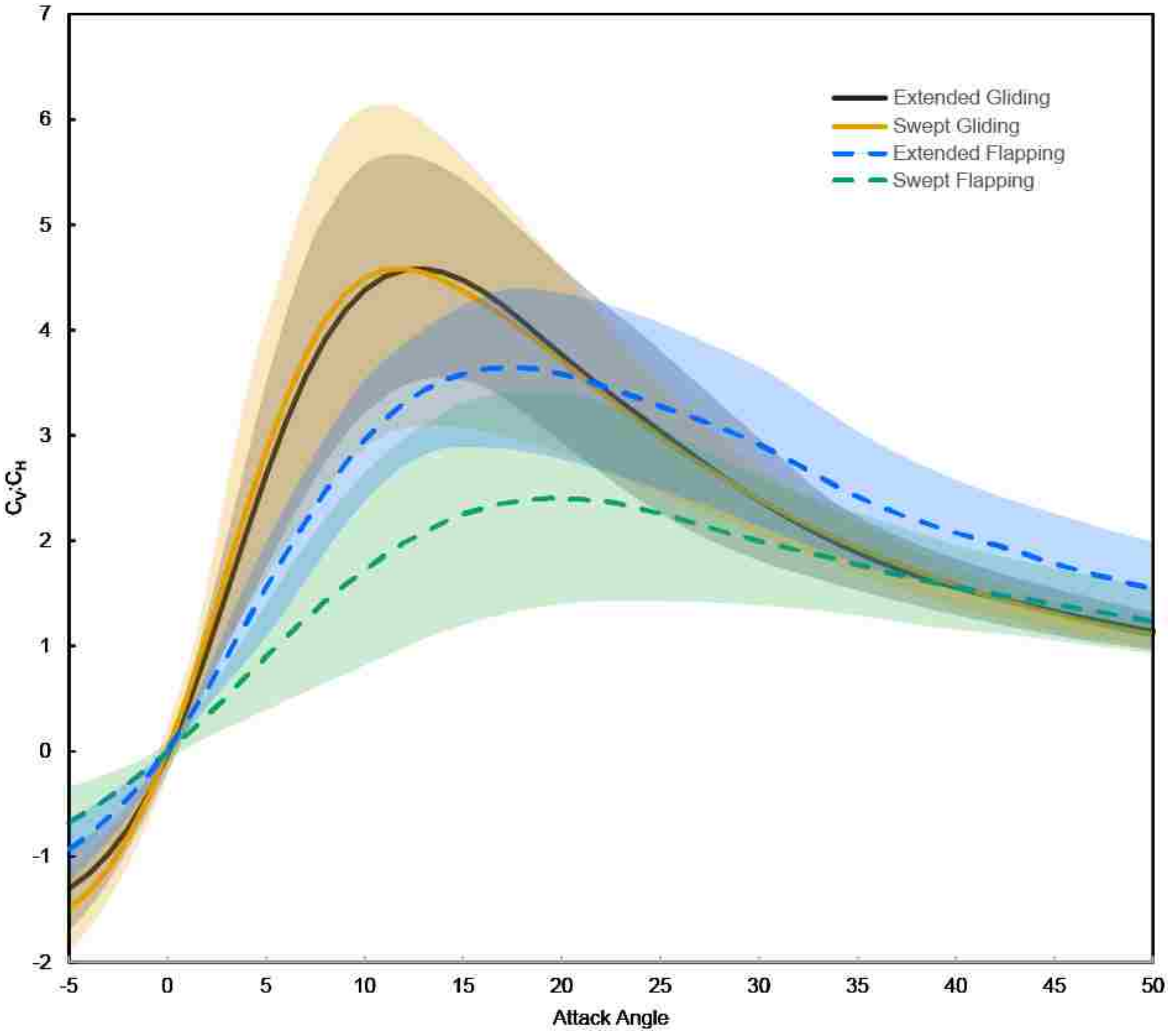

Figure 4: Mean vertical force coefficient (C_V) as a function of mean horizontal force coefficient (C_H) for wings of 13 raptor species. Error bars indicate ± SD for C_V and C_H.

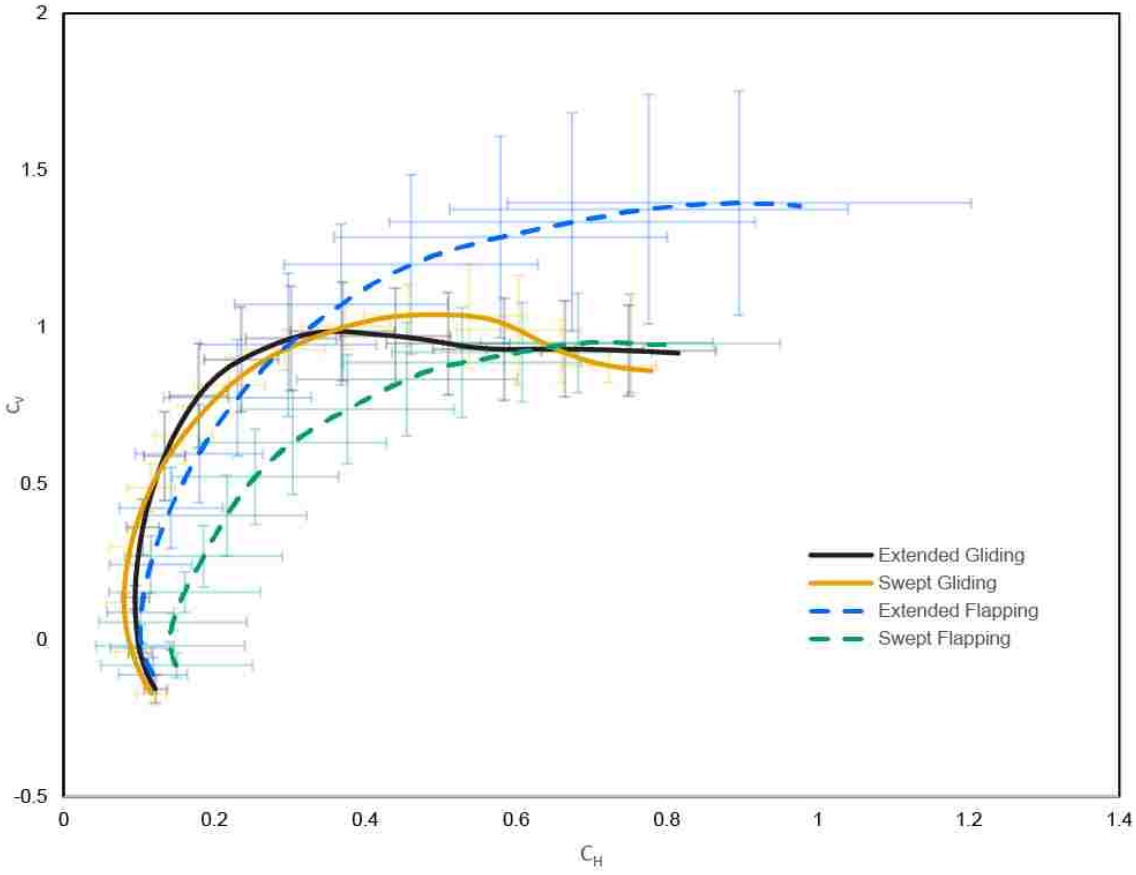

Figure 5: C_V as a function of attack angle in extended and swept postures during emulated flapping and gliding. The shaded regions represent ± SD.

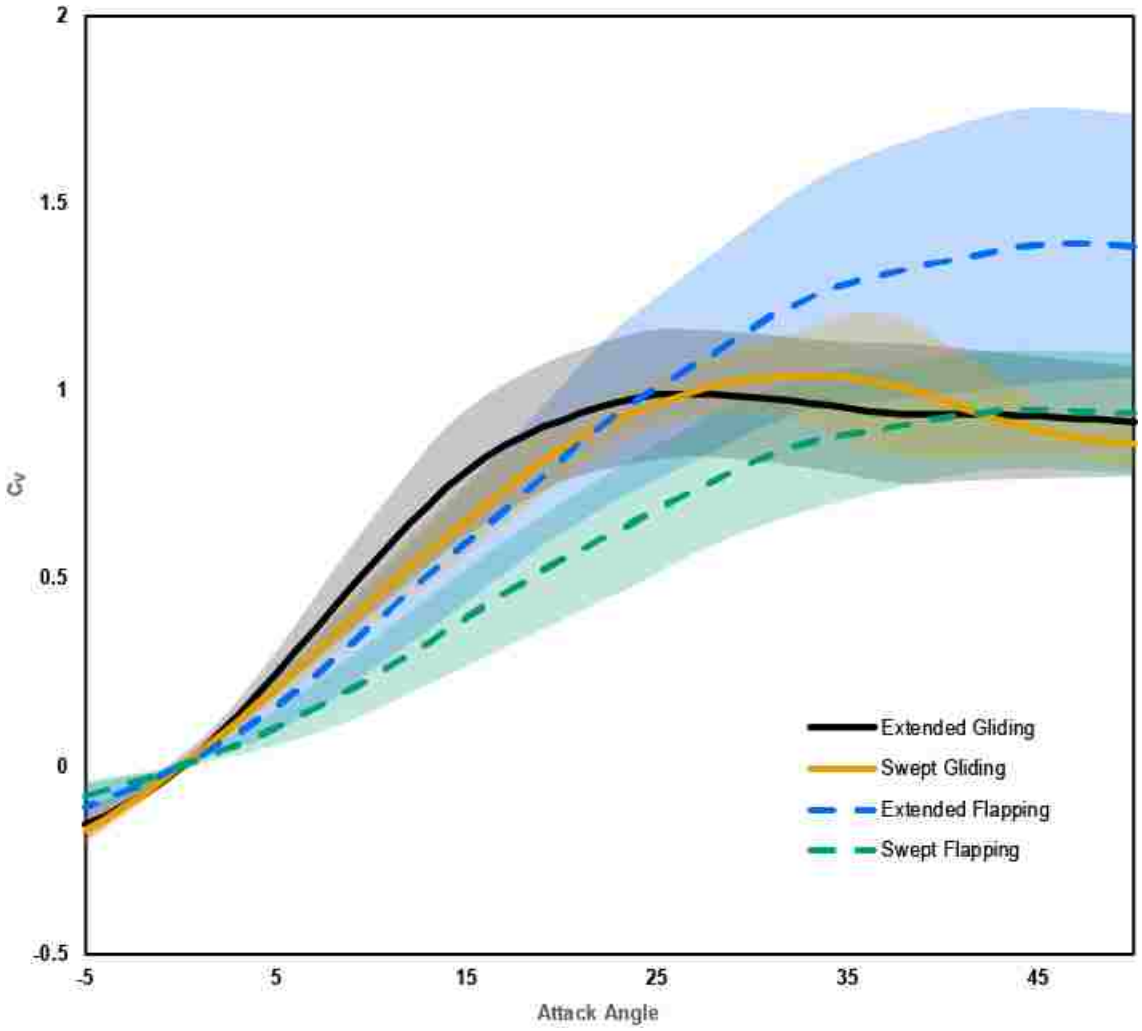

Figure 6: Individual polars of C_V as a function of C_H for wings of 13 raptor species configured in extended and swept postures and either spun as a propeller to emulate flapping flight or mounted in a wind tunnel to emulate gliding flight.

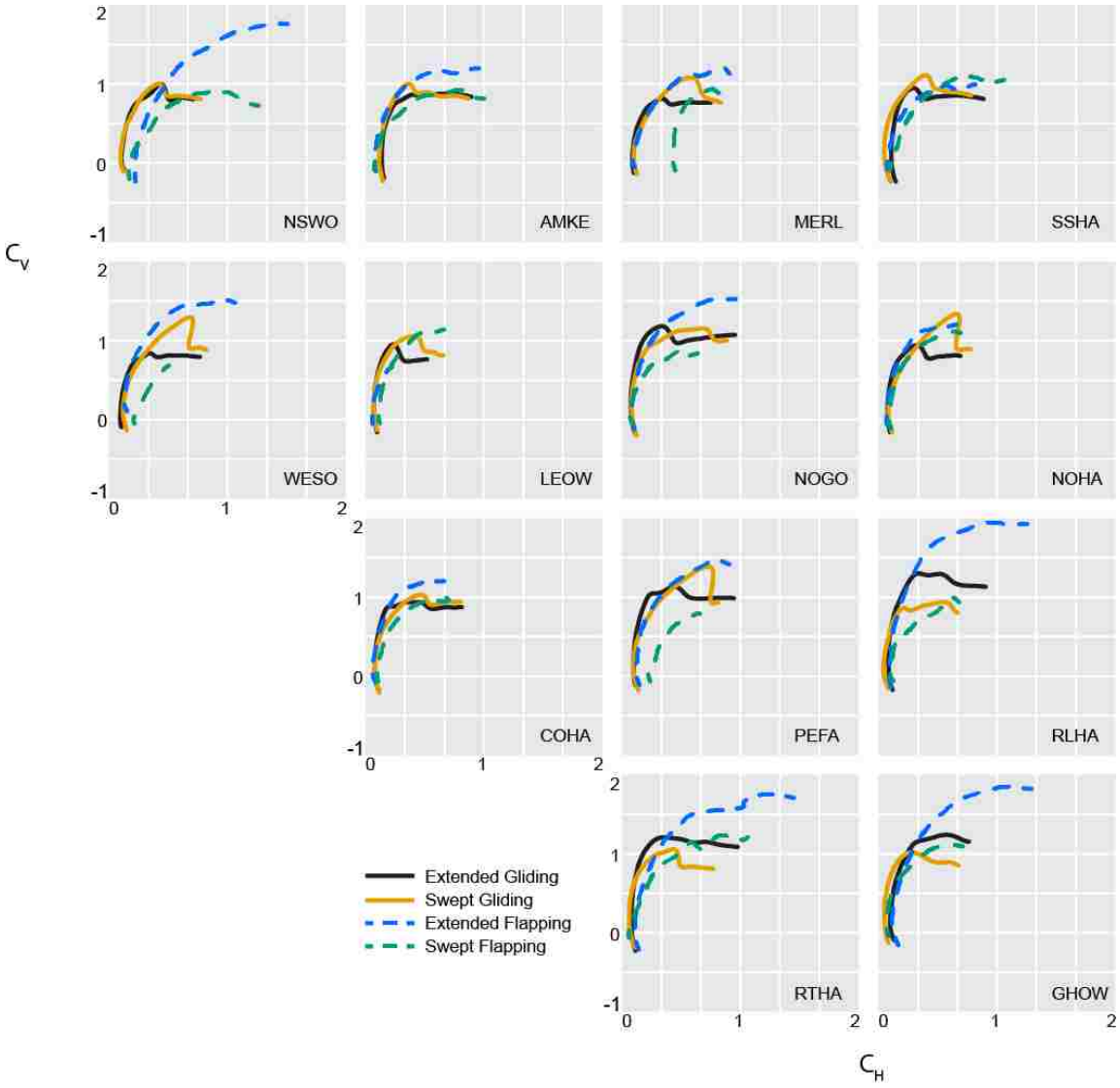

PHYLOGENETICS AND ECOMORPHOLOGY

OF EMARGINATE PRIMARY FEATHERS

AUTHORS: Brett Klaassen van Oorschot, Ho Kwan Tang, Bret W. Tobalske

ABSTRACT

Wing tip slots are a distinct morphological trait broadly expressed across the avian clade, but are generally perceived to be unique to soaring raptors. These slots are the result of emarginations on the distal leading and trailing edges of primary feathers, and allow the feathers to behave as individual airfoils. Research suggests these emarginate feathers are an adaptation to increase glide efficiency by mitigating induced drag in a manner similar to aircraft winglets. If so, we might expect birds known for gliding and soaring to exhibit emarginate feather morphology; however, that is not always the case. Here, we explore emargination across the avian clade, and examine associations between emargination and ecological and morphological variables. Pelagic birds exhibit pointed, high-aspect ratio wings without slots, whereas soaring terrestrial birds exhibit prominent wing-tip slots. Thus, we formed four hypotheses: (1) Emargination is segregated according to habitat (terrestrial, coastal/freshwater, pelagic). (2) Emargination is positively correlated with mass. (3) Emargination varies inversely with aspect ratio and directly with wing loading and disc loading. (4) Emargination varies according to flight style, foraging style, and diet. We found that emargination falls along a continuum that varies with habitat: Pelagic species tend to have zero emargination, coastal/freshwater birds have some emargination, and terrestrial species have a high degree of emargination. Among terrestrial and coastal/freshwater species, the degree of emargination is positively correlated with mass. We infer this may be the result of selection to mitigate induced power requirements during

slow flight that otherwise scale adversely with increasing body size. Since induced power output is greatest during slow flight, we hypothesize that emargination may be an adaptation to assist vertical take-off and landing rather than glide efficiency as previously hypothesized.

INTRODUCTION

The morphological variation found in the natural world can provide important information about how organisms locomote. Flight is an energetically expensive form of locomotion, and birds are highly adapted to fly both effectively (e.g. quick take off) and efficiently (e.g. increased glide ratio). Therefore, bird wing morphology is an ideal trait for which to evaluate the myriad constraints and selective pressures associated with flight. Variation in wing morphology is extraordinary, both in terms of overall wing shape as well as feather shape. Understanding this variation can provide key insight into how birds move through the fluid medium of air.

Wing tip slots are one aspect of wing morphology subject to significant variation. These slots are a common but varied morphological trait across the avian clade. Slotted wing tips are the result of missing "notches" or emarginations on the distal primary feathers (Fig. 1a, 1b). These emarginations are present on the leading and trailing edges of primary feathers, and allow the distal tips of these feathers to act as individual airfoils. Overall wing tip morphology and function are affected by the degree of emargination present in these primary feathers, but the aerodynamic role of these notches remain unclear.

Two functional hypotheses for emarginate primary feathers have been proposed: 1) emargination increases soaring efficiency by reducing induced drag (Trowbridge, 1906;

Tucker, 1993, 1995), and 2) emargination reduces the tendency for wing tip stall because the feathers can twist independently to decrease their angle of attack (Graham, 1932; Kokshaysky, 1973; Withers, 1981a, 1981b). Furthermore, it has been proposed that in concert with low aspect ratio wings, emarginate primary feathers may improve take-off performance and maneuverability (Pennycuick, 2008; Klaassen van Oorschot et al., 2016).

Testing these non-mutually exclusive hypotheses is challenging because efforts to experimentally modify the wing tip (e.g. removing feathers or filling in wing tip slots; see Tucker, 1995, and Withers 1981a, respectively) introduce new variables that confound the results. Therefore, to better understand the function of emarginate primary feathers, we took a new approach here by examining patterns of emargination across the avian clade and testing for correlations to ecological parameters of diet, flight style, and foraging behavior.

Casual observation suggests that primary feather emargination correlates with habitat. Terrestrial birds that are adept at thermal and orographic soaring (e.g. vultures, hawks; see Bohrer et al., 2011) have extremely slotted wing tips with emarginate primary feathers. In contrast, pelagic birds such as albatrosses, eminently capable of dynamic soaring, lack emarginate feathers altogether (Sachs et al., 2013). If slotted wing tips enhance soaring efficiency, why don't all soaring birds exhibit this morphology?

It may be that the selective pressures acting on wing tip morphology are more nuanced, complex, and species-specific than what aerodynamic theory alone suggests. Previous research by Tucker (1993, 1995) showed that emarginate primary feathers reduced drag in a gliding Harris's hawk, but more recent work contradicts these findings. A study exploring the wake behind a gliding jackdaw (*Corvus monedula*) showed that

vertically separated primary feathers did not significantly affect efficiency (KleinHeerenbrink et al., 2016). A recent study of swept and extended wings with emarginate feathers showed that lift and drag coefficients (aerodynamic force per unit wing area) were virtually the same during emulated gliding flight, but varied significantly in emulated flapping flight and were predominantly mediated by changes in lift (Klaassen van Oorschot et al., 2016). Conversely, a study exploring wings in emulated gliding flight showed that interspecific differences in wing morphology led to changes in aerodynamic performance that were predominantly due to profile drag (Lees et al., 2016). Combined, these findings indicate that the functional roles of wing tip shape and the emarginate primary feathers are still unclear. Rather than a simple aerodynamic explanation, there is likely a suite of ecological demands such as diet, flight style, and foraging behavior that act on morphological adaptation of the wing tip. Due to the complex and challenging locomotive behaviors exhibited by birds (e.g. takeoff, landing, soaring, gliding, maneuvering) and the wide range of ecological conditions they inhabit, it seems probable that efficiency during forward translational flight is only one selective pressure acting on wing tips.

To explore the potential factors that may be influencing primary feather emargination, we focused on several ecological, behavioral, and morphological parameters. Wing morphology and ecology have previously been linked in a variety of contexts including habitat type and migration (e.g. Lockwood et al., 1998; Bowlin and Winkler, 2004; Kaboli et al., 2007; Huber et al., 2016), but no studies have yet explored the potential links between emarginate primary feathers and ecology in a comprehensive phylogenetic context. These ecological parameters include flight style (soaring,

continuous flapping, dynamic soaring, flap/gliding, partial bounding, intermittent flap-bounding), foraging behavior (aerial, diving, gleaning, ground, skimming, soaring, swooping), and diet (carnivorous, herbivorous, omnivorous).

We also explored the morphological parameters of body mass, wing loading (weight divided by wing area, Eq. 1), wing length, aspect ratio (*AR*, the ratio of the square of wingspan to wing area, Eq. 2), and disc loading (weight divided by 360° wing sweep area, Eq. 3) to test for scaling relationships and/or tradeoffs that may explain emargination. Long, high-*AR* wings are generally hypothesized to be highly efficient during gliding whereas short, low-*AR* wings are thought to offer more maneuverability due to the lower moment of inertia of shorter wings. *AR* and wing length are associated with migration (both positively, see Bowlin and Winkler, 2004; and negatively, see Huber et al., 2016) and it is hypothesized that emargination may increase efficiency to allow for shorter, lower-*AR* wings (Tucker, 1993). High wing loading is better for high-speed flight because smaller wings produce less profile drag, whereas low wing and disc loading are best for slow-speed flight, such as takeoff and landing, because they minimize induced drag. The power required for hovering flight decreases with the square of disc loading (Ellington, 1984; Marden, 1987). Thus, in all species, but especially in those with high disc loading, emargination may be an adaptation to help mitigate the high power requirements of takeoff.

We used a phylogenetic, comparative approach to explore primary feather emargination across the avian clade. We measured the four distal-most primary feathers of 135 bird species and tested for correlations between emargination and independent variables. We provided an index for measuring and comparing feather emargination across taxa of various sizes. Previous research as well as anecdotal evidence led us to hypothesize

that 1) emargination is segregated according to habitat, 2) body mass is positively correlated with emargination, 3) emargination varies inversely with *AR* and directly with wing loading or disc loading, and 4) emargination is linked to the ecological variables of flight style, foraging style, and diet. We aimed to provide novel inferences regarding the selective pressures influencing emarginate primary feather morphology. More specifically, we wanted to determine if there is a continuum of primary feather emargination that varies from the pointed wing tips of pelagic birds to the slotted wing tips of terrestrial soaring birds.

METHODS

Specimens

We measured the four distal-most primary feathers of 135 species from 52 families of birds (Table S1). We utilized high-resolution images obtained from the United States Fish and Wildlife Service Forensic Laboratory's Feather Atlas (USFWS, 2010) for 118 species. We also measured feathers from 17 dried-wing specimens at the Slater Museum of Natural History at the University of Puget Sound, WA, USA. These specimens represent a wide variety of primarily North American species in diverse ecological and phylogenetic clades.

Morphometrics

We analyzed feather images using ImageJ (Schneider et al., 2012) and the ObjectJ plugin (https://sils.fnwi.uva.nl/bcb/objectj/) to calculate an emargination index for each species (see *Emargination Index* below). For dried-wing specimens, we performed the same measurements using a metric ruler. Measurement error was approximately ±0.5 mm

for both ImageJ and metric ruler measurements due to image resolution and ruler precision, respectively. For all species, we calculated whole-wing area and length within ImageJ using images of spread wings made available from the collection of the Slater Museum of Natural History at the University of Puget Sound, Tacoma, WA. The mass of the specimens was either unknown or may have been spurious due to unknown causes (e.g. dehydration before collection), so we used average sex-specific masses taken from Dunning (1992). When the sex of the specimen was unknown, we used average values based on both sexes.

We calculated three flight-related parameters to assess the relationship between emargination and flight performance. We calculated wing loading by multiplying wing area by two because we only had access to individual wings:

$$wing\ loading = \frac{mass}{area*2} \quad \text{Eq. 1}$$

Aspect ratio (*AR*) represents the ratio of square of wing length to wing area:

$$aspect\ ratio = \frac{length^2}{area} \quad \text{Eq. 2}$$

Disc loading is the ratio of the weight of the bird to the total area swept by the wings, assuming 360° rotation:

$$disc\ loading = \frac{mass * g}{\pi * length^2} \quad \text{Eq. 3}$$

Emargination Index

To quantify the amount of slotting present in the wing tip, we developed an emargination index (E) by measuring the four most distal primary feathers and calculating:

$$\mathrm{E} = \sum_{P_{\mathrm{d}-3}}^{P_{\mathrm{d}}} \frac{l_{\mathrm{slot}}}{l_{\mathrm{vane}}} \times \frac{c_{\mathrm{base}}}{c_{\mathrm{slot}}} \qquad \text{Eq. 4}$$

Where l_{slot} is the average of the distal leading and trailing edge slot lengths, l_{vane} is the total length of the feather vane, c_{base} is the chord of the base, c_{slot} is the chord of the slot and P_{d} is the distal-most primary feather (Fig. 1b). Chord values were measured at the widest points for both the base and slot feather sections. In cases where there was no emargination on the leading edge (i.e. P10) we used the trailing edge slot length alone. We summed the emargination of all four distal primary feathers to arrive at E. An E of zero indicates that there is no slotting present. As the amount of slotting increases, E increases concomitantly. This index provides a quantifiable metric for assessing the degree of slotting across species of various sizes.

Ecomorphological and Behavioral Parameters

We quantified foraging style, diet, and habitat type according to Erlich et al. (1988) (Foraging style: *aerial, diving, ground, skimming, soaring, swooping, gleaning*; Diet: *insects, fish, seeds, birds, omnivorous, small vertebrates, greens*; Habitat type: *terrestrial, coastal/freshwater, pelagic*). To explore gross differences in diet, we grouped specimens as omnivorous, herbivorous, or carnivorous based on their primary food sources. Flight styles were based on Bruderer et al. (2010) (*continuous flapping, soaring, dynamic soaring,*

flapping and long gliding, flapping and short gliding, partial bounding, and passerine-type, flap-bounding flight).

Phylogenetic and statistical analyses

To account for phylogenetic non-independence, we used phylogenetically corrected statistical models. We generated a majority rules consensus (MRC) tree based on 100 random trees taken from the posterior distribution of Jetz et. al. (2012) obtained from birdtree.org. The MRC tree was built using the APE package (Paradis, 2012) within R (R Core Team, 2015). To test for significant effects of categorical variables (habitat, diet, flight style, and foraging style) upon emargination, we analyzed phylogenetically corrected generalized least squares models (pGLS) built using the nlme R package (Pinheiro et al., 2016). We used Akaike's information criterion (AIC) to select the best models, and found that a Brownian motion model of evolution yielded the best fit for all statistical tests. We performed analysis of variance tests on the pGLS models which are presented in Table 1. We calculated pseudo R-squared values for the pGLS models using linear models of the actual dependent variables and the fitted model dependent variables. We excluded wing area, *AR*, wing loading, disc loading, and wing length as interaction terms because they are confounded with mass and did not improve the fit of the statistical models. In cases where two continuous variables were compared (i.e. aspect ratio, wing loading, disc loading, emargination, or mass), we computed phylogenetically independent contrasts (PIC, Felsenstein, 1985; Paradis, 2012). These PICs were then used in linear models fit through the origin (PIC-lm, Wilkinson and Rogers, 1973; Chambers, 1992). We found that pelagic birds had very little or no emargination regardless of mass, so for clarity we omitted them from our PIC-lm graphs (Fig. 4) (see Table 3a). Herein we report means

± standard deviation (S.D.) for emargination, and means ± standard error (S.E.) for slopes and scaling exponents. Since the body mass of the species in our sample spanned several orders of magnitude (6 grams to 11,100 grams), we normalized all morphometric data by using a base-10 log transformation. We transformed the emargination index using base-10 log+1 to avoid taking the log of zero.

RESULTS

Primary feather emargination was present in 98 of the 135 species sampled (73%). Feather emargination was strongly influenced by both mass (*m*) and habitat type. Birds that regularly fly over land (i.e. terrestrial and coastal/freshwater species) exhibited increasing emargination as a function of *m* (Fig. 2a). In contrast, pelagic species had zero or nearly zero emargination across *m*. Sixty-five of the 71 terrestrial (T) species (92%), 32 of 38 coastal/freshwater (CFW) species (84%), and 1 of 26 pelagic (P) species (4%) exhibited primary feather emargination (Fig. 2b). Terrestrial and coastal/freshwater species had similar mean emargination indices (T: 1.82±1.15, CFW: 1.49±1.14), and both were significantly greater than pelagic species (P: 0.02±0.11; $p<0.001$, $F_{(2,\ 129)}=13.44$, pGLS, Fig. 2b, Table 1 & 2).

Phylogeny also had an effect upon mean emargination and habitat group (Fig. 3 & 4). Of the 71 terrestrial species, 67 (94%) shared a single basal node in the tree we used for analysis. With the exception of five species that are known for fast flight and maneuvering during aerial capture of insects (swifts, swallows, martins, and nighthawks) and the rock dove (*Columba livia*), all of these taxa (65 species) had emarginate primary

feathers. In contrast, coastal and freshwater species were intermixed with pelagic species throughout the phylogeny.

The golden eagle (*Aquila chrysaetos*) had the most emargination (E=4.65) among all birds in the study. Both pelican species (*Pelecanus erythrorhynchos* and *Pelecanus occidentalis*), classified as coastal/freshwater, exhibited noteworthy emargination (E=3.80 and 3.72, respectively). The only pelagic species with emargination was the brown booby (*Sula leucogaster*, E=0.58).

After accounting for phylogeny, terrestrial birds exhibited feather emargination that scaled $\propto m^{0.13\pm0.03}$ ($p<0.0001$ $R^2=0.20$, PIC-lm, Fig. 4a, Table 3a). For coastal and freshwater species, $E \propto m^{0.19\pm0.05}$ ($p<0.001$, $R^2=0.15$, PIC-lm, Fig. 4a, Table 3a). Emargination of pelagic species did not scale significantly with mass ($p=0.91$, $R^2=-0.04$, PIC-lm, Table 3a). Emargination scaled $\propto$ area$^{0.15\pm0.04}$ for terrestrial birds ($p<0.001$, $R^2=0.14$, PIC-lm) and $\propto$ area$^{0.27\pm0.07}$ for coastal and freshwater species ($p<0.001$, $R^2=0.31$, PIC-lm; Fig. 4b, Table 3a). Emargination scaled $\propto$ wing loading$^{0.26\pm0.07}$ for terrestrial birds ($p<0.001$, $R^2=0.15$, PIC-lm) but not for coastal/freshwater species or pelagic species ($p>0.05$ for both, Fig. 4c, Table 3a). Emargination scaled $\propto$ disc loading$^{0.28\pm0.06}$ for terrestrial species ($p<0.05$, $R^2=0.22$, PIC-lm) but did not scale $\propto$ disc loading in coastal/freshwater species ($p=0.35$) or pelagic species ($p=0.83$, PIC-lm, Fig. 4d, Table 3a). Emargination scaled $\propto AR^{-0.38\pm0.17}$ for terrestrial species ($p=0.03$, $R^2=0.05$, PIC-lm) but no relationship was observed for coastal/freshwater species ($p=0.98$, $R^2=-0.03$, PIC-lm) or pelagic species ($p=0.85$, $R^2=-0.04$, Fig. 4e, Table 3a). Non-phylogenetically controlled results are available in Table 3b.

Behavioral and ecological factors

Flight style was a significant predictor of emargination ($p<0.01$, $F_{(6, 128)}=3.12$, pGLS, Fig. 5c, Table 1). Soaring birds had higher emargination (E=3.4±1.17) than other species and dynamic soaring birds had lower emargination (E=0.0±0.0). Foraging style and diet did not have significant effects upon E ($p>0.3$ for all, pGLS, Table 1). As general trends, soaring foragers had the highest average E, while skimming birds had the lowest (Fig. 5a, Table 2). Carnivores had slightly lower E than herbivores or omnivores (Fig. 5b, Table 2). Finally, habitat was a significant predictor of *AR* and wing length ($p<0.001$ and 0.03, pGLS, Figs. 6, 7, Table 1). Pelagic species had significantly higher *AR* than coastal/freshwater or terrestrial species. Wing length tracked closely with body mass, but terrestrial species had wings that were 46% shorter than pelagic and coastal/freshwater species. (Table 2, Fig. 7).

DISCUSSION

Our results provide evidence in a comparative, phylogenetic framework that emarginate feathers are a common morphological feature among terrestrial and coastal/freshwater birds. Primary feather emargination falls along a continuum where birds that fly almost exclusively over water have almost no emargination, birds that fly in coastal/freshwater zones have some emargination, and birds that fly exclusively over land have the most emargination (Fig. 2a, 2b). In contrast, whole-wing *AR* follows an inverse pattern: pelagic species have high-*AR* wings, coastal/freshwater species have intermediate *AR*, and terrestrial species have the lowest *AR* (Fig. 6). Emargination, when present,

increased with body mass, wing area, wing loading, and disc loading. Primary feather emargination and *AR* may therefore represent a functional tradeoff in wing design that is modulated by habitat-specific aeroecological factors. These findings provide novel insight into the evolution and function of emarginate primary feathers.

Why don't all birds have slotted primary feathers?

There are distinct differences in the aerial habitats of terrestrial, coastal/freshwater, and pelagic birds that have likely allowed each group to evolve different wing morphologies. Pelagic birds experience relatively constant surface winds, and many of the pelagic species in our study capitalize on reliable trade-winds (Weimerskirch et al., 2000; Shaffer et al., 2001; Suryan et al., 2008). By taking off into a headwind, these birds are able to bypass some of the costly slow-speed flight required to reach cruising velocity. Even at a groundspeed of zero, a head wind can produce positive air speed before takeoff and therefore reduce the energy required to transition from slow to fast flight. The most costly aspects of flight for wandering albatrosses (and indeed, all birds) are take-offs and landings, and albatrosses avoid take-offs during periods of calm winds (Weimerskirch et al., 2000; Shaffer et al., 2001). The long wings of many pelagic species may make flapping flight relatively costly as the inertial work required for flapping increases exponentially with wing length (van den Berg and Rayner, 1995). Pelagic birds tend to use flap-gliding, swell soaring, and/or ground effect to minimize power costs (Alerstam et al., 1993). The long wings of pelagic species may perform exceptionally poorly during take-off in no wind when wingbeat amplitude and inertial costs are highest.

In contrast, terrestrial species regularly experience zero to highly variable wind when taking off from the ground due to the presence of a near-ground atmospheric

boundary layer (Warrick et al., 2016). that may be more unpredictable than over water because of surface roughness (e.g. grasses) and obstructions (e.g. trees, shrubs), so that even when strong winds prevail in the freestream, a calm breeze may not be felt within a few meters above the ground (Garratt, 1994). Moreover, terrestrial birds must be able to quickly ascend vertically to avoid predation and negotiate three-dimensional habitat (e.g. grasses, rocks, trees) not common in the pelagic environment. With less help from predictable maritime head winds, terrestrial species are likely under strong selective pressures to produce maximal aerodynamic forces during takeoff and landing while minimizing the inertial costs of vigorous flapping. It has been proposed that low aspect-ratio wings with slotted feathers are adapted for performance during take-off and maneuvering rather than for gliding (Pennycuick, 2008; Klaassen van Oorschot et al., 2016) and the results of the present study support this hypothesis.

Why does emargination increase with mass, wing loading, and disc loading?

Birds face physical and physiological constraints associated with flight that become more costly with size. The mass-specific induced power requirement (induced power per unit body mass) for flight is proportional to $m^{1/6}$ (Pennycuick, 1975; Wakeling and Ellington, 1997). That is, as birds get larger, proportionally more power is required to produce weight support. Additionally, the mass-specific power available for flight decreases with $m^{-1/6}$ to $m^{-1/3}$ (Hill, 1950; Pennycuick, 1975; Ellington, 1991; Altshuler et al., 2010; Jackson and Dial, 2011). These physical and physiological scaling relationships pose significant constraints on bird flight, with easily observed declines in flight performance as body size increases among species. High wing loading and disc loading only exacerbate the problem of additional mass, as wings are smaller or shorter for a given

mass, respectively, and either trend should increase induced power output. Our results suggest that the evolution of emargination may have been in response to the selective pressure of induced power requirements during take-off, landing, and slow flight—a pressure that scales adversely with increasing mass and is increased via high wing loading and disc loading.

Most of the outliers in this study provide further support for the hypothesis that slotted feathers are predominantly used to maximize force production during slow flight. Terrestrial birds with no emargination tended to be fast fliers (e.g. swifts, martins, swallows) that do not land on the ground, and can therefore take off by first descending from a high perch to gain speed. Conversely, coastal/freshwater species with considerable emargination were large (e.g. pelicans, swans, wood stork), and slotted primary feathers may help them take off with heavy body masses and/or prey. One pelagic species, the brown booby (*Sula leucogaster*), exhibited a small amount of emargination (0.58) on the trailing edge of P10. A closely related species, the red-footed booby (*Sula sula*), exhibited no emargination. It is unclear why the brown booby showed some emargination. Additionally, many coastal/freshwater species such as coots, sandpipers, and avocets had low emargination values. These species may also utilize head winds associated with the coastal/freshwater habitat, and also frequently use low-angle take-off trajectories to minimize power costs.

Emargination and ecology

We hypothesized that emargination is related to flight style, foraging style, and diet. If this were true, we could conclude that emargination may be a product of factors associated with their behavior rather than habitat or aeroecological conditions. We found that soaring and dynamic soaring were the only two factors that correlated with emargination. This could be because these flight styles are tightly linked with habitat and mass—soaring and dynamic soaring birds are generally heavy and live in terrestrial or pelagic habitat, respectively. These birds may be at the edges of maximum size for their specific ecological niches, and may therefore be highly specialized for their specific aerial habitats and behaviors. For example, dynamic soaring species with no emargination live exclusively in habitats with regular maritime winds. These species are freed from the constraints of slow flight during takeoff and landing due to the presence of headwinds. As such, their long, tapered wings are highly adapted for efficiency during high-speed translational flight. Conversely, terrestrial soaring birds must take-off regularly from the ground and often fly as slowly as possible to benefit from thermal updrafts. In these conditions, emarginate primary feathers may enhance lift and reduce induced drag costs which dominate at slow speeds (Hoerner, 1965).

Foraging style and diet did not correlate with emargination. We had small sample sizes in each foraging type. For example, birds that skimmed water for prey had zero emargination, but the sample size in this group (n=8) limited statistical power. Diet was a poor predictor all-around because every diet group had species with mixed levels of emargination.

Emargination presents itself in different ways across the phylogeny, yet appears follows a universal pattern of feather shape, beginning at the distal tip with notch width generally increasing proportionally with total feather length. Our index "E" does not capture the full diversity of primary feather shapes and should be interpreted as a coarse metric. For example, owls and corvids exhibit similar values of E, but owls tend to have short, wide notches at the trailing-edge tips of the distal primary feathers. In contrast, corvids have notches that are longer and thinner and occupy both the leading and trailing edges of the feathers.

Conclusions

Primary feather emargination has traditionally been considered a trait for efficient soaring (Trowbridge, 1906; Tucker, 1993, 1995), but many of the world's soaring birds (i.e. pelagic seabirds) have zero emargination. We found that emargination was associated with terrestrial and coastal/freshwater habitat, and positively correlated with mass. Emargination also increased as a function of disc loading and wing loading but decreased with *AR*. Therefore, we hypothesize that emargination evolved in response to directional selection associated with the adverse scaling of induced power requirements during slow flight such as takeoff and landing. Headwinds expedite the transition from slow to fast flight, and tradewinds are a common feature in pelagic habitat. Thus, the emarginate primary feathers of terrestrial birds may be adaptations to minimize the induced power costs of takeoff in little or variable wind.

ACKNOWLEDGEMENTS

We thank Paige Folsom, Ondi Crino, Kileen Marshall, Sara Smith, Natalie Wright, Pepper Trail, Brian Crego, Teresa Feo, Brenda Miller, the USFWS Forensics Laboratory, and the Slater Museum of Natural History for their support and assistance.

FUNDING

This research was supported by National Science Foundation grants GRFP DGE-1313190 to B.K.v.O. and IOS-0923606, IOS-0919799 and CMMI 1234747 to B.W.T

REFERENCES

Alerstam T, Gudmundsson GA, Larsson B. 1993. Flight tracks and speeds of Antarctic and Atlantic seabirds: Radar and optical measurements. Philos Trans R Soc B Biol Sci 340:55–67.

Altshuler DL, Dudley R, Heredia SM, McGuire JA. 2010. Allometry of hummingbird lifting performance. J Exp Biol 213:725–734.

Bohrer G, Brandes D, Mandel JT, Bildstein KL, Miller TA, Lanzone M, Katzner T, Maisonneuve C, Tremblay JA. 2011. Estimating updraft velocity components over large spatial scales: Contrasting migration strategies of golden eagles and turkey vultures. Ecol Lett 15:1–8.

Bowlin MS, Winkler DW. 2004. Natural variation in flight performance is related To timing of breeding in tree swallows (Tachycineta bicolor) in New York. Auk 121:345–353.

Bruderer B, Peter D, Boldt A, Liechti F. 2010. Wing-beat characteristics of birds recorded with tracking radar and cine camera. Ibis 152:272–291.

Chambers JM, Hastie T. 1992. Linear models. 1st ed., Statistical Models in S. Pacific Grove, CA: Wadsworth & Brooks/Cole. 624 p.

Dunning Jr. JB. 1992. CRC Handbook of avian body masses. 2nd ed. Boca Raton, FL: CRC Press. 672 p.

Ellington C. 1991. Limitations on animal flight performance. J Exp Biol 91:71–91.

Ellington CP. 1984. The Aerodynamics of Hovering Insect Flight. III. Kinematics. Philos Trans R Soc B Biol Sci 305:41–78.

Erlich PR, Dobkin DS, Wheye D. 1988. The birder's handbook: A field guide to the natural history of North American birds. New York: Simon & Schuster.

Felsenstein J. 1985. Phylogenies and the Comparative Method. Am Nat 125:1–15.

Garratt JR. 1994. Review: the atmospheric boundary layer. Earth-Science Rev 37:89–134.

Graham RR. 1932. Safety devices in wings of birds. Aeronaut J 36:24–58.

Hill AV. 1950. The dimensions of animals and their muscular dynamics. Sci Prog 38:209–230.

Hoerner SF. 1965. Fluid-dynamic Drag. Bakersfield, CA: Hoerner Fluid Dynamics. 455 p.

Huber GH, Turbek SP, Bostwick KS, Safran RJ. 2016. Comparative analysis reveals migratory swallows (Hirundinidae) have less pointed wings than residents. Biol J Linn Soc.

Jackson BE, Dial KP. 2011. Scaling of mechanical power output during burst escape flight in the Corvidae. J Exp Biol 214:452–461.

Jetz W, Thomas GH, Joy JB, Hartmann K, Mooers AO. 2012. The global diversity of birds in space and time. Nature 491:444–448.

Kaboli M, Aliabadian M, Guillaumet A, Roselaar CS, Prodon R. 2007. Ecomorphology of the wheatears (genus Oenanthe). Ibis 149:792–805.

Klaassen van Oorschot B, Mistick EA, Tobalske BW. 2016. Aerodynamic consequences of wing morphing during emulated take-off and gliding in birds. J Exp Biol 219:3146–3154.

KleinHeerenbrink M, Warfvinge K, Hedenström A. 2016. Wake analysis of aerodynamic components for the glide envelope of a jackdaw (Corvus monedula). J Exp Biol 219:1572–1581.

Kokshaysky N V. 1973. Functional aspects of some details of bird wing configuration. Syst Zool 22:442–450.

Lees JJ, Dimitriadis G, Nudds RL. 2016. The influence of flight style on the aerodynamic properties of avian wings as fixed lifting surfaces. PeerJ 4:e2495.

Lockwood R, Swaddle JP, Rayner JMV. 1998. Avian wingtip shape reconsidered: wingtip shape indices and morphological adaptations to migration. J Avian Biol 29:273–292.

Marden JH. 1987. Maximum lift production during takeoff in flying animals. J Exp Biol 130:235–238.

Paradis E. 2012. Analysis of Phylogenetics and Evolution with R. 2nd ed. New York: Springer-Verlag. 386 p.

Pennycuick CJ. 1975. Mechanics of flight. J Avian Biol 5:1–75.

Pennycuick CJ. 2008. Modelling the flying bird. 1st ed. London: Academic Press. 1-479 p.

Pinheiro J, Bates D, DebRoy S, Sarkar D, R Core Team. 2016. nlme: linear and nonlinear mixed effects models.

R Core Team. 2015. R: A language and environment for statistical computing.

Sachs G, Traugott J, Nesterova A, Bonadonna F. 2013. Experimental verification of dynamic soaring in albatrosses. J Exp Biol 216:4222–4232.

Schneider CA, Rasband WS, Eliceiri KW. 2012. NIH Image to ImageJ: 25 years of image analysis. Nat Methods.

Shaffer SA, Costa DP, Weimerskirch H. 2001. Behavioural factors affecting foraging effort

of breeding wandering albatrosses. J Anim Ecol 70:864–874.

Spedding GR, McArthur J. 2010. Span efficiencies of wings at low Reynolds numbers. J Aircr 47:120–128.

Suryan RM, Anderson DJ, Shaffer SA, Roby DD, Tremblay Y, Costa DP, Sievert PR, Sato F, Ozaki K, Balogh GR, Nakamura N. 2008. Wind, waves, and wing loading: Morphological specialization may limit range expansion of endangered albatrosses. PLoS One 3:e4016.

Trowbridge CC. 1906. Interlocking of emarginate primary feathers in flight. Am J Sci 21:145–169.

Tucker VA. 1993. Gliding birds: reduction of induced drag by wing tip slots between the primary feathers. J Exp Biol 180:285–310.

Tucker VA. 1995. Drag reduction by wing tip slots in a gliding Harris' hawk, Parabuteo unicinctus. J Exp Biol 198:775–781.

USFWS. 2010. Feather Atlas [WWW Document]. URL https://www.fws.gov/lab/featheratlas/

van den Berg C, Rayner J. 1995. The moment of inertia of bird wings and the inertial power requirement for flapping flight. J Exp Biol 198:1655–1664.

Wakeling JM, Ellington CP. 1997. Dragonfly flight III. Lift and power requirements. J Exp Biol 200:557–582.

Warrick DR, Hedrick TL, Biewener AA, Crandell KE, Tobalske BW, Warrick DR. 2016. Foraging at the edge of the world : low-altitude, high-speed manoeuvering in barn swallows. Philos Trans R Soc B 371:20150391.

Weimerskirch H, Guionnet T, Martin J, Shaffer SA, Costa DP. 2000. Fast and fuel efficient? Optimal use of wind by flying albatrosses. Proc Biol Sci 267:1869–1874.

Wilkinson GN, Rogers CE. 1973. Symbolic descriptions of factorial models for analysis of variance. Appl Stat 392–399.

Withers PC. 1981a. An aerodynamic analysis of bird wings as fixed aerofoils. J Exp Biol 90:143–162.

Withers PC. 1981b. The aerodynamic performance of the wing in red-shouldered hawk (Buteo linearis) and a possible aeroelastic role of wing-tip slots. Ibis 123:239–247.

TABLES

Table 1. Results of analysis of variance of pGLS models

Model	Model terms	D.F.	F-statistic	Pseudo R-squared	P-value
Log(E) ~ Habitat * Log(mass)	Habitat	2, 129	13.44	.67	**<0.001**
	Log(mass)	1, 129	26.67		**<0.001**
	Habitat * Log(mass)	2, 129	5.90		**<0.01**
Log(E) ~ Flight Style * Log(mass)	Flight style	6, 121	3.22	.24	**<0.01**
	Log(mass)	1, 121	13.88		**<0.001**
	Flight style * Log(mass)	6, 121	0.46		0.8
Log(E) ~ Flight Style + Log(mass)	Flight style	6, 127	3.46	.26	**<0.01**
	Log(mass)	1, 127	14.9		**<0.001**
Log(E) ~ Foraging Style * Log(mass)	Foraging style	6, 121	1.32	.09	0.3
	Log(mass)	1, 121	14.63		**<0.001**
	Foraging style * Log(mass)	6, 121	0.90		0.5
Log(E) ~ Foraging Style + Log(mass)	Foraging style	6, 127	1.39	.05	0.2
	Log(mass)	1, 127	15.3		**<0.001**
Log(E) ~ Diet * Log(mass)	Diet	2, 129	0.65	.05	0.5
	Log(mass)	1, 129	16.76		**<0.001**
	Diet * Log(mass)	2, 129	0.30		0.7
Log(E) ~ Diet + Log(mass)	Diet	2, 129	0.65	.05	0.5
	Log(mass)	1, 129	16.76		**<0.001**
Log(*AR*) ~ Habitat * Log(mass)	Habitat	2, 129	8.05	.50	**<0.001**
	Log(mass)	1, 129	0.03		0.9
	Habitat * Log(mass)	2, 129	3.65		**0.03**
Log(L) ~ Habitat * Log(mass)	Habitat	2, 129	3.57	.89	**0.03**
	Log(mass)	1, 129	167.58		**<0.001**
	Habitat * Log(mass)	2, 129	2.93		**<0.01**

Table 2. Average primary feather emargination by ecological group

E ~ Habitat Type	E mean ± SD
Terrestrial	1.82±1.15
Coastal/Freshwater	1.49±1.14
Pelagic	0.02±0.11

E ~ Flight Style	E mean ± SD
Continuous flapping	1.02±1.05
Soaring	3.40±1.17
Dynamic soaring	0.06±0.19
Flap/glide long	1.29±1.25
Flap/glide short	1.06±0.34
Partial bounding	0.00±0.00
Intermittent flap-bounding	1.46±0.59

E ~ Foraging Style	E mean ± SD
Aerial	1.37±1.12
Diving	1.14±1.22
Gleaning	1.11±0.30
Ground	1.46±1.06
Skimming	0.00±0.00
Soaring	2.88±1.89
Swooping	1.56±0.79

E ~ Diet	E mean ± SD
Carnivore	1.24±1.32
Herbivore	1.76±0.73
Omnivore	1.55±1.16

Aspect Ratio (*AR*) ~ Habitat	*AR* mean ± SD
Terrestrial	2.24±0.62
Coastal/Freshwater	2.99±0.57
Pelagic	4.12±0.84

Wing Length (L) ~ Habitat	L mean ± SD
Terrestrial	0.23±0.19
Coastal/Freshwater	0.42±0.24
Pelagic	0.44±0.20

TABLE 3a. Phylogenetic linear models of morphological variables by habitat group

PIC-lm	Group	slope	d.f.	R-squared	F-statistic	p-value
log(E) ~ log(mass)	T	0.13±0.03	1,69	0.20	18.80	**<0.0001**
	CFW	0.19±0.05	1,36	0.15	13.06	**<0.001**
	P	0.002±0.02	1,24	-0.04	0.01	0.91
log(E) ~ log(area)	T	0.15±0.04	1,69	0.14	12.43	**<0.001**
	CFW	0.27±0.07	1,36	0.31	17.75	**<0.001**
	P	0.003±0.03	1,24	-0.04	0.00	0.99
log(E) ~ log(wing loading)	T	0.26±0.07	1,69	0.15	13.74	**<0.001**
	CFW	0.17±0.17	1,36	0.00	0.97	0.33
	P	0.01±0.03	1,24	0.00	0.04	0.84
log(E) ~ log(disc loading)	T	0.28±0.06	1,69	0.22	20.71	**<0.0001**
	CFW	0.15±0.16	1,36	0.00	0.89	0.35
	P	0.006±0.03	1,24	-0.04	0.05	0.83
log(E) ~ log(*AR*)	T	-0.38±0.17	1,69	0.05	4.99	**<0.05**
	CFW	-0.01±0.36	1,36	-0.03	0.00	0.98
	P	-0.02±0.09	1,24	-0.04	0.04	0.85

TABLE 3b. Non-phylogenetic linear models of morphological variables by habitat group

non-PIC lm	Group	slope	intercept	d.f.	R-squared	F-statistic	p-value
log(E) ~ log(mass)	T	0.15±0.02	0.11±0.05	1,69	0.36	39.85	**<0.0001**
	CFW	0.28±0.04	-0.48±0.12	1,36	0.57	51.75	**<0.0001**
	P	0.02±0.02	-0.03±0.05	1,24	-0.01	0.69	0.15
log(E) ~ log(area)	T	0.20±0.03	0.78±0.06	1,69	0.35	38.61	**<0.0001**
	CFW	0.37±0.05	0.85±0.07	1,36	0.58	52.42	**<0.0001**
	P	0.02±0.02	-0.03±0.03	1,24	-0.02	0.52	0.48
log(E) ~ log(wing loading)	T	0.38±0.09	0.21±0.05	1,69	0.21	19.6	**<0.001**
	CFW	0.24±0.11	0.12±0.11	1,36	0.09	4.62	**0.04**
	P	0.02±0.03	-0.004±0.03	1,24	-0.03	0.24	0.63
log(E) ~ log(disc loading)	T	0.40±0.08	0.02±0.08	1,69	0.28	27.68	**<0.0001**
	CFW	0.27±0.12	0.004±0.16	1,36	0.09	4.75	**0.04**
	P	-0.01±0.003	0.00±0.003	1,24	-0.04	0.07	0.8
log(E) ~ log(*AR*)	T	-0.38±0.20	0.54±0.07	1,69	0.04	3.72	0.06
	CFW	0.17±0.37	0.27±0.18	1,36	-0.02	0.22	0.65
	P	0.06±0.09	-0.03±0.06	1,24	-0.02	0.48	0.5

FIGURES

Figure 1a: Distal primary feathers of four characteristic species exhibiting varying degrees of emargination: RTHA: red-tailed hawk (*Buteo jamaicensis*), E=3.95; GHOW: great horned owl (*Bubo virginianus*), E=1.61; LAGU: laughing gull (*Larus atricillia*), E=0; LTDU: long-tailed duck (*Clangula hyemalis*), E=1.01. These are representative of many species in the study. (Images courtesy of the USFWS Forensic Laboratory Feather Atlas.)

Figure 1b: The emargination index (E, Eqn. 1) is the sum of four measurements from each of the four primary feathers: c_{base} is the chord of the feather base, c_{slot}, is the chord of the feather slot, l_{vane} is the length of the whole feather vane, and l_{slot} is the average length of the leading and trailing slots.

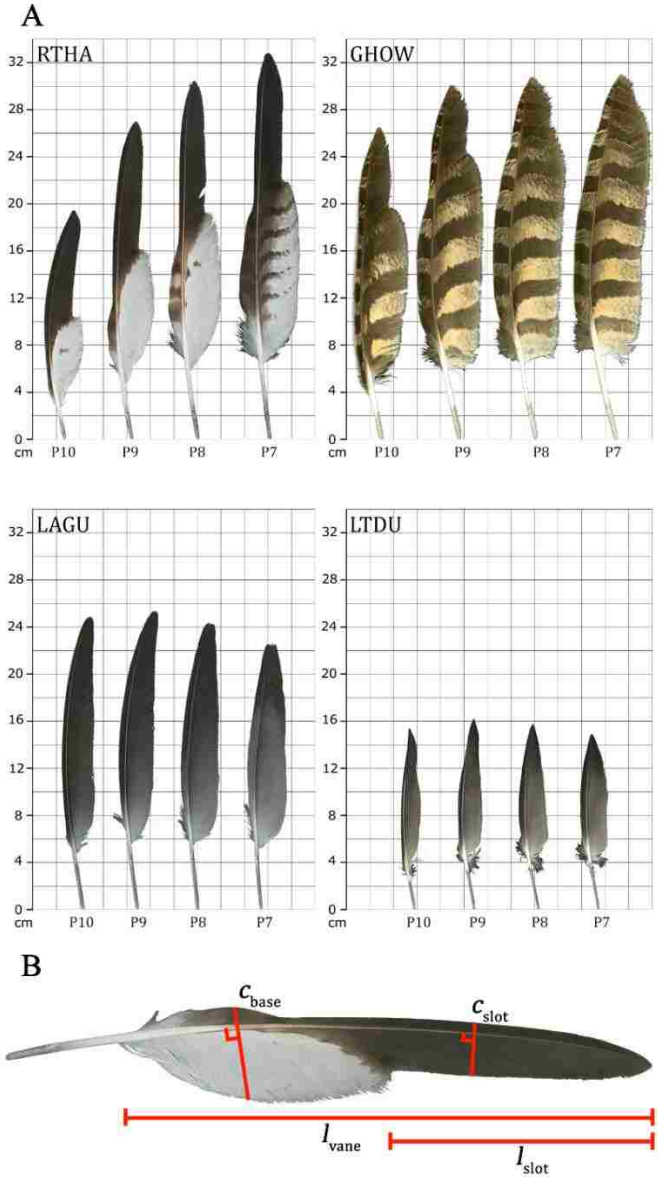

Figure 2a: Primary feather emargination (E) is influenced by mass (*m*) in terrestrial species and coastal/freshwater species, but does not change in pelagic species. Terrestrial: $E=m^{0.15}+0.11$; Coastal/Freshwater: $E=m^{0.29}-0.48$; Pelagic: $E=m^{0.02}-0.03$.

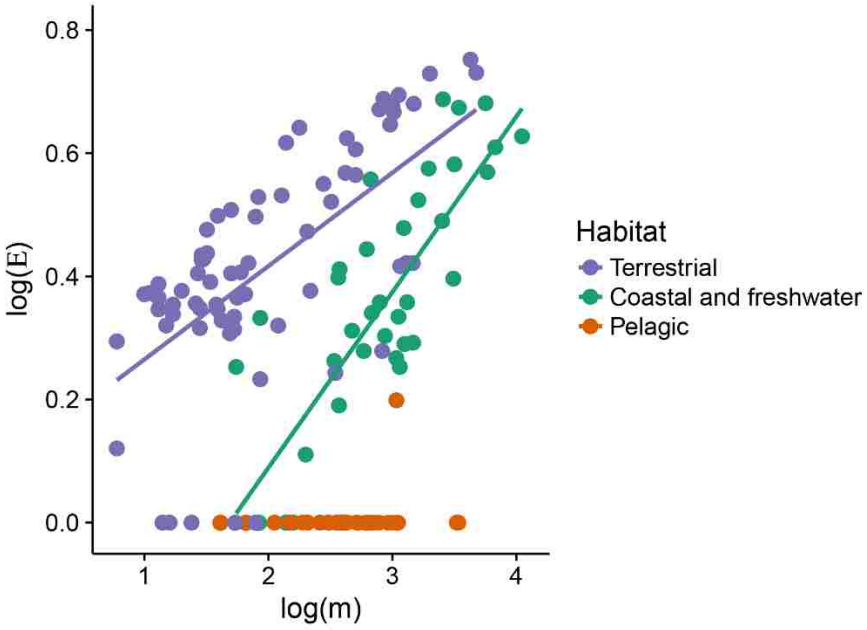

Figure 2b: Coastal/freshwater and terrestrial species have significantly more feather emargination (E) than pelagic species ($p<0.0001$, pGLS). Terrestrial: E=1.82±1.15; Coastal/freshwater: E=1.49±1.14; Pelagic: E=0.02±0.11. Black lines indicate mean ± 1 S.D.

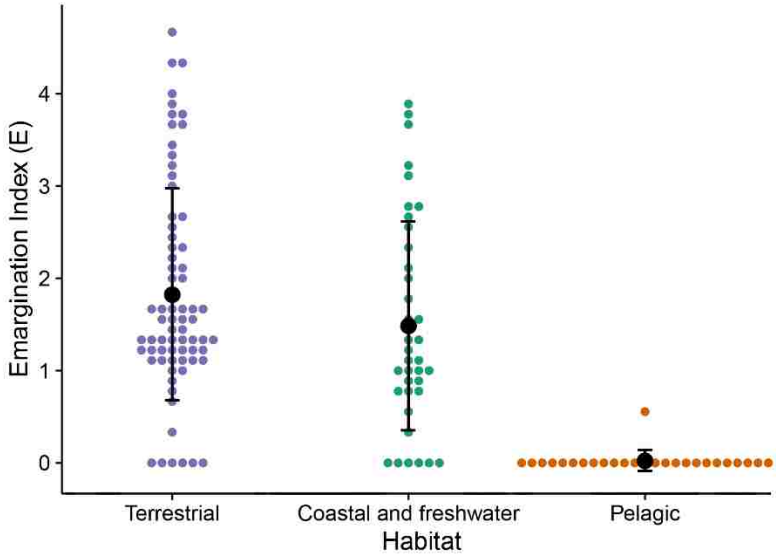

Figure 3: Majority rules consensus (MRC) tree of 135 avian species. Species names are colored by habitat, and emargination is shown for each.

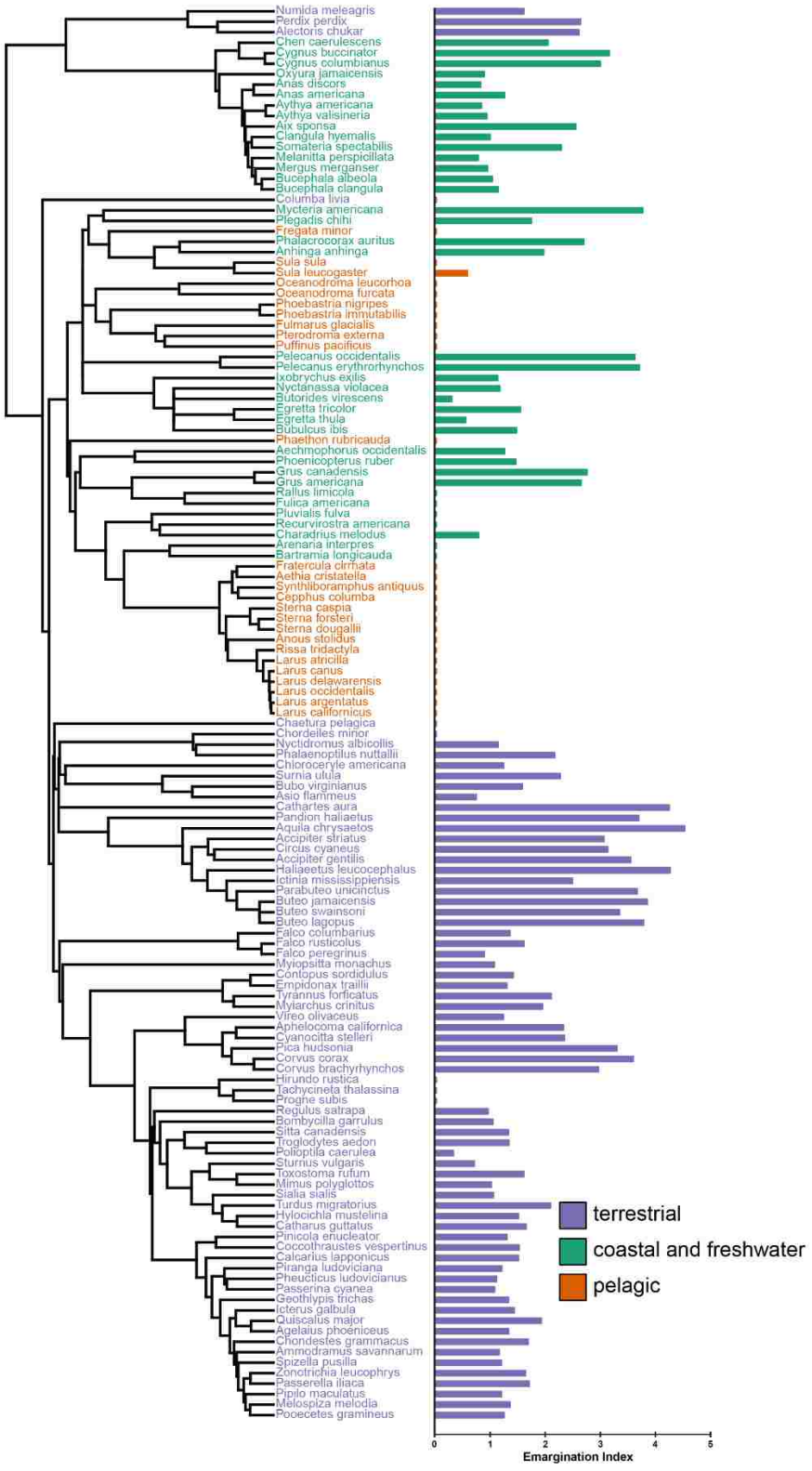

Figure 4: Linear models for phylogenetically independent contrasts show emargination positively scales with mass (A), area (B), wing loading (C), and disc loading (D), and scales negatively with aspect ratio (E). Terrestrial: solid line; Coastal/freshwater: dashed line; Pelagic omitted because no model significantly fit. See Table 3a for statistics.

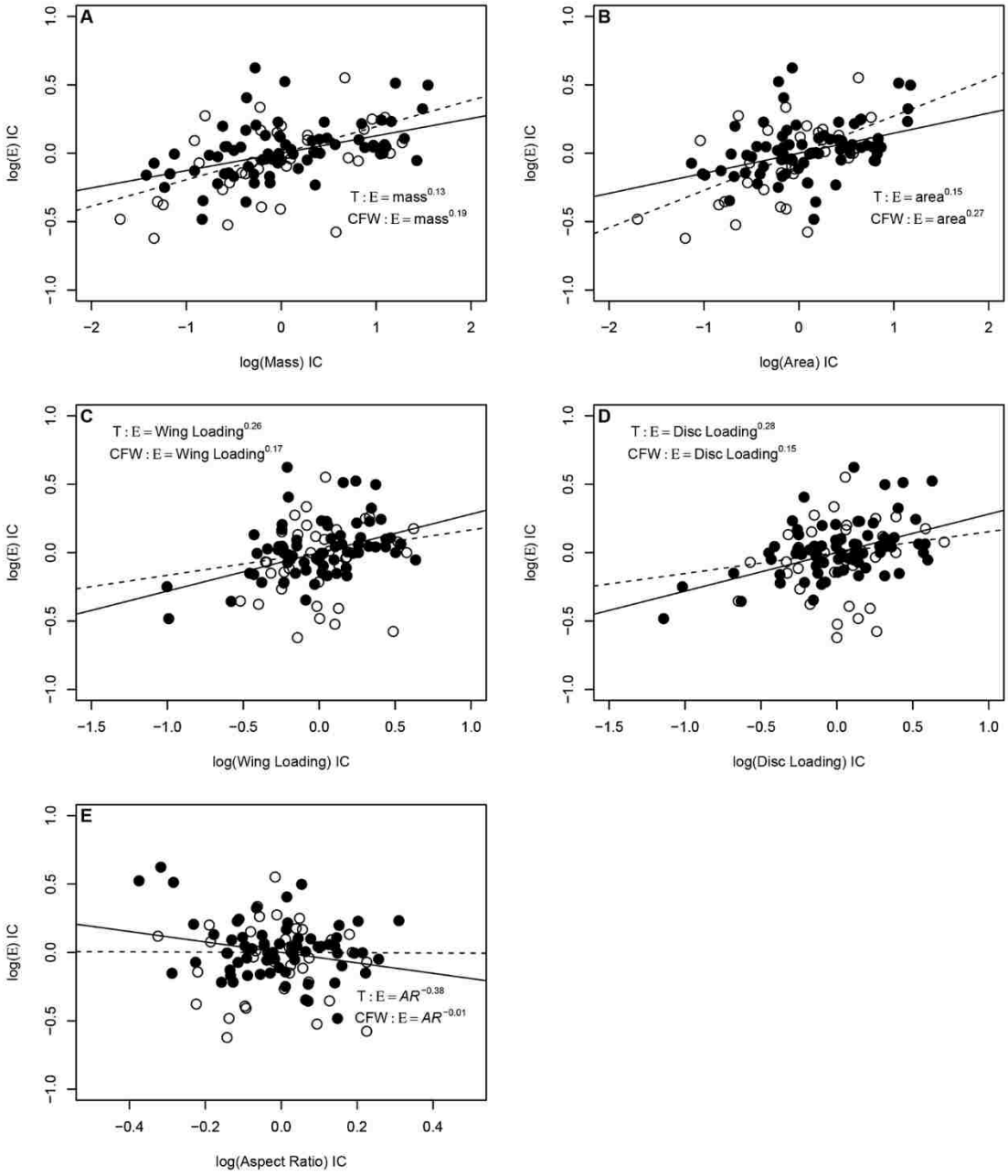

Figure 5: Foraging style (A) and diet (B) were not significant predictors of emargination. Flight style, however, did significantly influence emargination (C). Black lines indicate mean ± 1 S.D. See Table 2 for statistics.

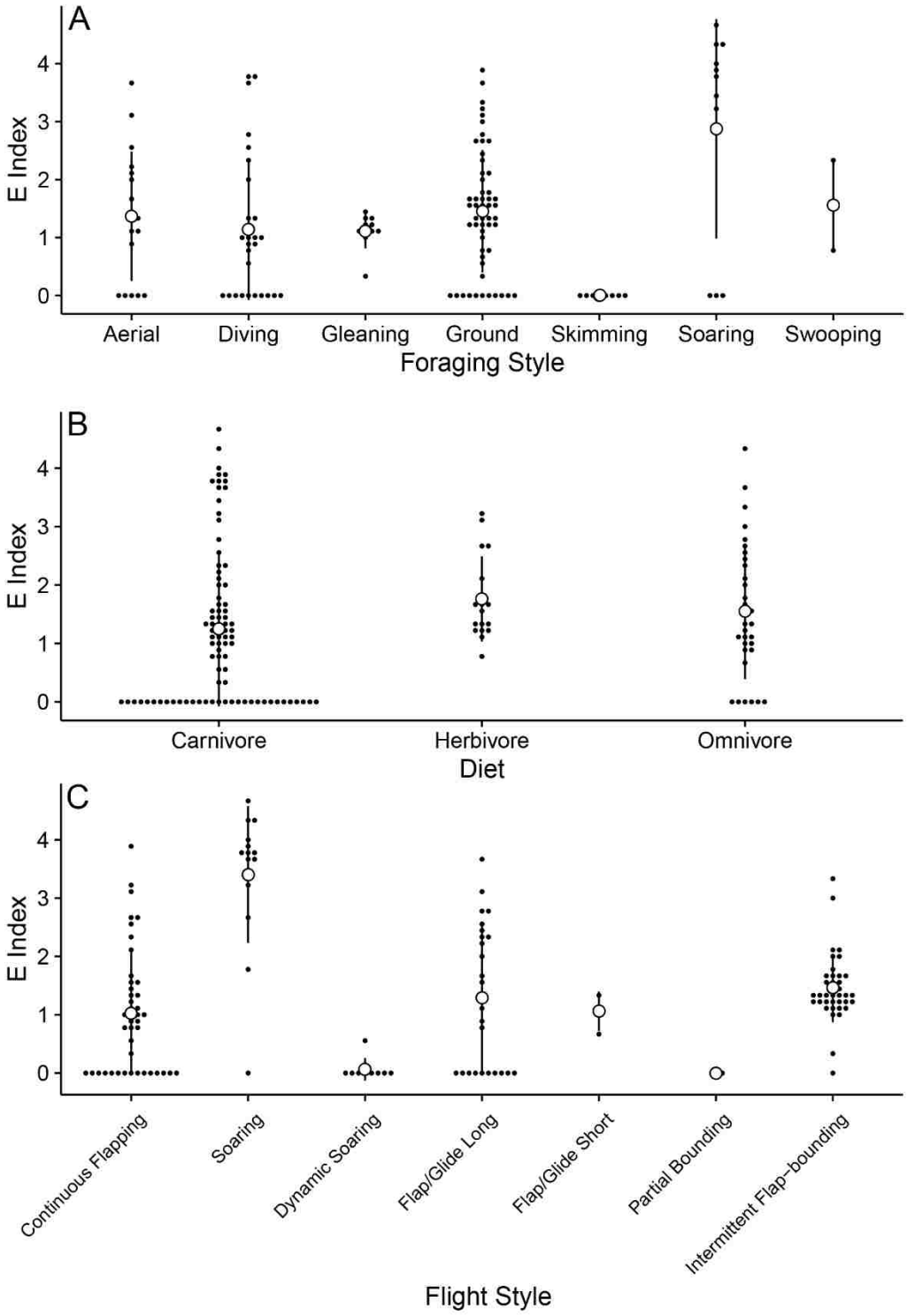

Figure 6: Wing aspect ratio is influenced by habitat type and mass. Terrestrial birds have the lowest aspect ratios, coastal/freshwater birds have medium aspect ratios, and pelagic species have the highest aspect ratios. Aspect ratios in all three groups increase as a function of body mass. See Table 2 for statistics.

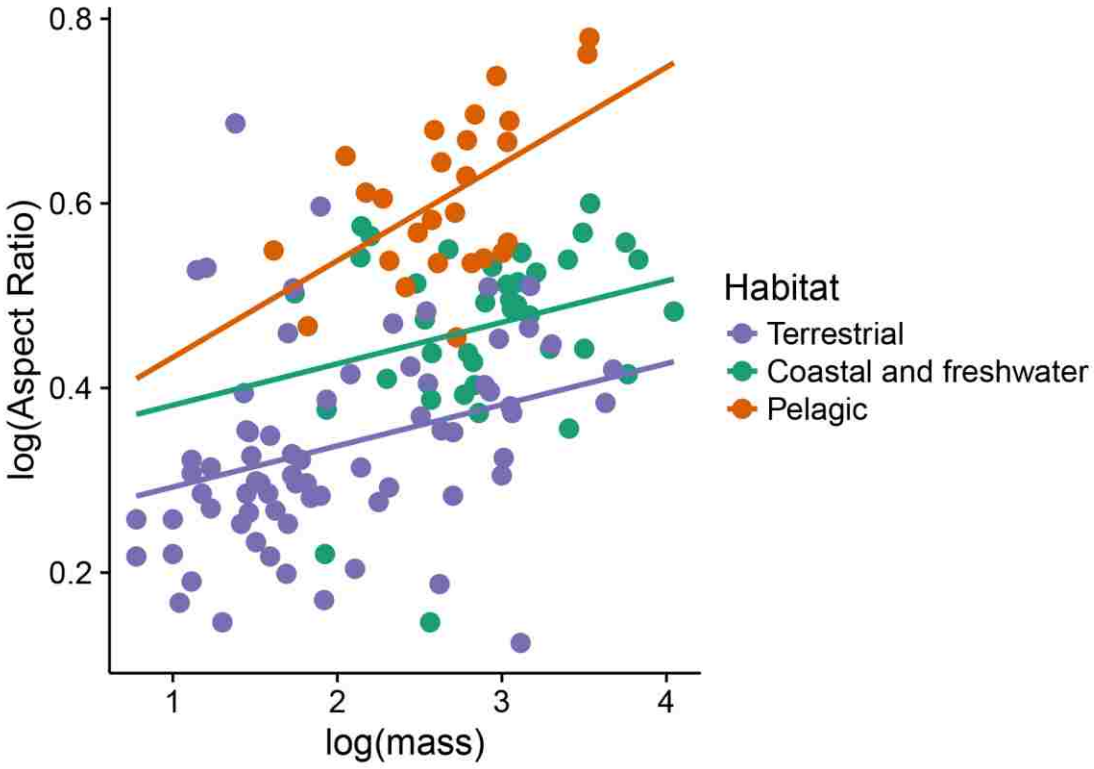

Figure 7: Wing lengths increase with mass. Terrestrial species had wings that were half as long as pelagic or coastal/freshwater species. See Table 2 for statistics.

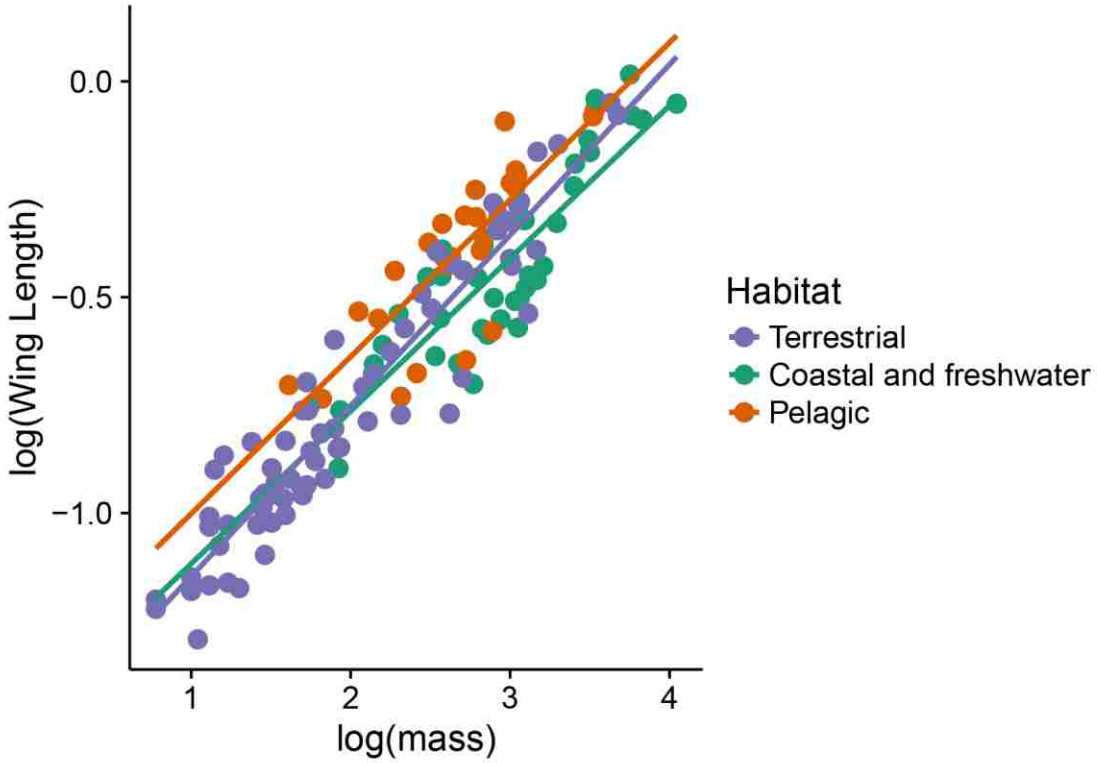

PASSIVE AEROELASTIC DEFLECTION OF AVIAN PRIMARY FEATHERS

AUTHORS: Brett Klaassen van Oorschot, Richard Choroszucha, Bret W. Tobalske

ABSTRACT

Bird feathers are complex structures that can passively deflect as they interact with air to produce aerodynamic force. Newtonian theory suggests that feathers should be stiff to efficiently transmit these forces back to the bird's body. However, *in vivo* observations indicate that feathers are flexible and deflect in response to airflow *via* bending, twisting, and sweeping. These deflections are hypothesized to optimize flight performance, but this has not yet been comprehensively evaluated. We examined primary feather deflection in a wind tunnel to explore how flexibility altered aerodynamic forces in emulated gliding flight. Using primary feathers from seven raptors and a Clark-Y airfoil, we quantified deflection, including bending, sweep, and twisting, as well as α (attack angle) and slip angle. We also quantified aerodynamic forces in all three axes. Based on previous research, we hypothesized that 1) feathers would deflect under aerodynamic load, 2) bending would result in lateral redirection of force, 3) twisting would alter α and delay the onset of stall, and 4) flexural stiffness of feathers would decrease with body mass. We found that bending resulted in the generation of lateral forces ~10% of total lift. In comparison to the Clark-Y airfoil which stalled at α=13.5°, all feathers continued to increase lift production beyond the range of measurements (α=27.5°). We attribute this difference to spanwise long-axis twist which reduced the local α at the feather tips. Additionally, flexural stiffness varied with mass$^{1.1}$, indicating that feathers get relatively more flexible with mass. These findings provide useful insight into the function of flexible

feathers, and suggest that flexibility provides passive roll stability and delays stall. Our findings are the first to quantify 3-D feather deflection and concomitant aerodynamic force, and can inform future models of avian flight as well as biomimetic morphing-wing technology.

INTRODUCTION

The avian wing is a remarkable adaptation that allows birds to locomote effectively and efficiently throughout a diverse range of aerial conditions. In contrast to the relatively inflexible wings of traditional aircraft, avian wings morph actively and passively in response to air flow to maximize performance (Sun et al., 2016). This flexibility is in part due to the numerous flexible feathers which comprise the wing and act as the principal aerodynamic surfaces involved in flight. Feathers passively deflect in response to flow as well as alter the flow itself, resulting in a complex interplay between aerodynamic, inertial, and mechanical forces (Pennycuick and Lock, 1976; Norberg, 1985; Rayner, 1988). This passive deflection appears to be highly tuned by evolutionary selection (Lingham-Soliar, 2014). Thus, feather deflection is hypothesized to confer performance benefits in terms of efficiency, lift production, and stability across flight modes (Norberg, 1985; Lindhe Norberg, 2002). Traditional aircraft have wings that are designed to perform best in a narrow range of the flight envelope (Barbarino et al., 2011; Sun et al., 2016). However, recent developments in smart materials and structures may allow aircraft designers to engineer wings with flexibility similar to feathers (e.g. Sun et al., 2016; Heo et al., 2011; Pankonien and Inman, 2014). This flexibility has the potential to improve stability and performance. Here, we examined the relationship between aerodynamic loading and

feather deflection during emulated gliding to determine the consequences of feather flexibility during flight.

Most birds have some degree of slotting at the wing tips that allow feathers to function as individual aerodynamic surfaces (Withers, 1981; Erlich et al., 1988; Tucker, 1993; Lockwood et al., 1998; Klaassen van Oorschot et al., 2017). In these feathers, asymmetric reductions in the leading and trailing vanes of the feathers provide separation for the feathers to bend, twist, and sweep independently. In species with slotted wing tips, *in vivo* observations show feathers often bend dorsally (vertically) during gliding, causing a dihedral wing tip (Trowbridge, 1906; Tucker, 1993, 1995; Carruthers et al., 2007). Historically, it has been hypothesized that these slotted feathers bend dorsally to function like winglets on an airplane, breaking up the wingtip vortex and increasing efficiency (Tucker, 1993, 1995). However, recent studies of whole-wing aerodynamics have shown that these feathers may not improve gliding flight efficiency (Klaassen van Oorschot et al., 2016; KleinHeerenbrink et al., 2016). Two alternative functional hypotheses have been proposed: 1) Feather slots allow individual feathers to bend dihedrally which increases lateral (also termed roll or spiral mode) stability by redirecting aerodynamic forces medially over the bird's center of gravity (Graham, 1932; Withers, 1981). 2) Feather slots allow individual feathers to twist which many enhance force production (i.e. lift and/or thrust) and reduce stall by minimizing the angle of attack (α) of each feather (Withers, 1981; Norberg, 1985; Fluck and Crawford, 2014). Meanwhile, sweep has been shown to reduce yawing moments in birds, thus improving yaw stability and pitch control (Taylor and Thomas, 2002; Sachs and Moelyadi, 2006).

Previous work has generally focused on whole-wing aerodynamics or adapted findings from aeronautical research to hypothesize on the function of these flexible feathers (Trowbridge, 1906; Graham, 1932; Tucker, 1993, 1995; Swaddle and Lockwood, 2003; Sachs and Moelyadi, 2006; Klaassen van Oorschot et al., 2016; KleinHeerenbrink et al., 2016). Based on aerodynamic theory, it is thought that feathers should be as stiff as possible to efficiently transmit aerodynamic force to the body (Corning and Biewener, 1998; Tubaro, 2016). However, passive deflection of primary feathers is well documented (Trowbridge, 1906; Carruthers et al., 2007). Feathers are presumably highly adapted to maximize aerodynamic performance, but we presently lack understanding of how deflection at the scale of individual feathers influences aerodynamics.

Empirical work on individual feather deflection has predominantly focused on feather shaft stiffness during static mechanical loading (Worcester, 1996; Bachmann et al., 2012; Wang et al., 2012). Worcester (1996) and Wang et al. (2012) show that larger birds have proportionally more flexible feathers than smaller birds, a finding that has been termed the "flexible shaft hypothesis" (see Pap et al., 2015). In these studies, feathers were measured by removing the barbs, fixing the calamus of the feather in place, and applying a point load along the rachis. Dorsal-ventral flexion (vertical bending) along one axis was measured to determine flexural stiffness of the feather. However, these studies do not consider the anisotropic nature of feather bending and ignore the three-dimensionality of deflection (i.e. twist and sweep). They also do not account for the complex loading of aerodynamic force or the potential contribution of the barbs in deflection. Purslow and Vincent (1978) kept the barbs intact, but otherwise used the same methodology to measure feather bending. They noted that their measurements of bending were likely systematically

reduced by some torsional deflection. Thus, the complex three-dimensional deflection and concomitant redirection of aerodynamic forces that primary feathers exhibit during gliding flight remain unknown.

While traditional aircraft designers have been slow to adopt morphing wing technology, the recent growth of micro air vehicles (MAV) can provide an ideal testbed for biomimetic morphing aerodynamics. Understanding the aerodynamics of flexible bird feathers may inform next-generation morphing MAV and full-size aircraft design (e.g. Graham, 1932; Bachmann et al., 2007; Barbarino et al., 2011; Fluck and Crawford, 2014; Sun et al., 2016). As new smart materials and structures are developed (e.g. Sofla et al., 2010), biomimetic application of feather morphing may become commonplace.

Here, we investigated how aerodynamic loading influenced three-dimensional feather deflection, and how that deflection influenced force production for primary feathers from seven raptor species. These species exhibit slotted primary feathers that experience freestream flow and routinely engage in flap-gliding or soaring flight (Erlich et al., 1988; Klaassen van Oorschot et al., 2017). We also used a rigid Clark-Y airfoil to compare aerodynamics of feather deflection to a similarly sized airfoil that does not deflect. We examined how feather deflection changes with α and velocity (V), and measured the force produced by the feathers during each treatment. We predicted that feathers would deflect in all three axes (bend, sweep, and twist) under aerodynamic load (Corning and Biewener, 1998; Bachmann et al., 2012; Fluck and Crawford, 2014). We also predicted that feather bending would reorient resultant forces laterally towards the midline of the bird (Thomas and Taylor, 2001), and that feather twist would delay the onset of stall compared to the airfoil (Brown, 1963; Norberg, 1985; Lindhe Norberg, 2002). Finally, we predicted feather

flexural stiffness (EI) would decrease with body mass (Worcester, 1996; Wang et al., 2012; Pap et al., 2015).

MATERIALS AND METHODS

Specimens

We utilized the right eighth primary feather (P8) from seven raptorial species (*Falco sparverius, Falco columbarius, Accipiter cooperii, Buteo jamaicensis, Falco peregrinus, Bubo virginianus, and Pandion haliaetus*) for deflection and force analysis, as well as a Clark-Y rigid foam airfoil (Rocketship Systems, Inc.; www.flyingfoam.com) as a comparison for force analysis only. The feathers were removed from specimens that had already died from causes unrelated to this study. We affixed the calamus of each feather to a 4-5mm hollow brass rod using Devcon 5-minute epoxy. For reference of α, we secured a small pushpin to each calamus just proximal to the downy barbs. Due to the extreme flexibility of the downy barbs at the proximal base of the feather, the pushpin was required to maintain an accurate proximal reference plane.

We used 2-mm dots of white paint with a center 1-mm black dot to mark five points along the feather, with the head of the pushpin representing a sixth point. We used these points to define position vectors and yield two planes which we used to quantify deflection (see '*Quantifying deflection*' below).

Force measurements and wind tunnel

We recorded feathers at 12 at-rest (i.e., without airflow, 0 m s^{-1}) geometric at-rest attack angles (α_{pre}, -22.5°<α_{pre}<+27°) in 3.5° increments and two velocities (*V*; 8 ms^{-1}, 12 ms^{-1}) in a wind tunnel at the Flight Laboratory at the University of Montana (Tobalske et al., 2005). At each α_{pre} and *V*, we collected force data at 1 kHz for several seconds and then filtered those force traces using a 3-Hz low-pass Butterworth filter before taking an average of the forces over the duration of the measurement. The feathers were held in place using a NEMA 23 stepper motor (23W108D-LW8, Anaheim Automation, Inc.) that was affixed to a custom-made force plate located outside of the wind tunnel (15×15 cm platform, 200-Hz resonant frequency; Bertec Corporation, Columbus, OH, USA). Each feather was initially set to α_{pre}=0° using a laser level at two-thirds of the feather's span. We then rotated the feathers using the stepper motor to change α. Drag associated with the brass rod into which the feather was mounted was subtracted from the total drag, and lift from the rod was assumed to be zero.

We evaluated aerodynamics of the feathers and airfoil by computing vertical, horizontal, and lateral force coefficients (C_V, C_H, C_K, respectively) using the following equations (from Usherwood and Ellington, 2002a):

$$C_V = \frac{2F_V}{\rho V^2 S} \qquad C_H = \frac{2F_H}{\rho V^2 S} \qquad C_K = \frac{2F_K}{\rho V^2 S} \qquad \text{(Eq. 1, 2, 3)}$$

where C_V is the coefficient of vertical force, C_H is the coefficient of horizontal force, C_K is the coefficient of lateral force, F_V is vertical force (N), F_H is the horizontal force (N), F_K is the lateral force (N), ρ is air density at Missoula, MT, (978 m elev., 1.07 kg/m^3), V is the velocity, and S is the projected area of the feather (m^2).

Quantifying deflection

To measure deflection as it related to α and V, we analyzed each feather at α_{pre}=0° and α_{pre}=13.5° and four Vs (0 ms^{-1}, 8 ms^{-1}, 12 ms^{-1}, 16 ms^{-1}). We recorded feather deflection using three Photron PCI 1024 video cameras (1024 x 1024 pixels) synchronized to frame via TTL pulse. The cameras recorded at 500 Hz with a 1/1000 s shutter speed. We then digitized the location markers on the feathers and reconstructed 3D coordinates using direct linear transformation (DLT) of the synchronized video with custom script in MATLAB (DLTdv5, Hedrick, 2008).

Treating the location markers as position vectors, we analyzed angles between two planes, proximal and distal, each described by two vectors comprised of points {1,2,3} and {4,5,6}, respectively (Fig. 1a, 1b).

The feathers were modeled as cantilever beams with the proximal end anchored at point 2 and the distal end free. The feather's natural shape at rest (0 ms^{-1}) was used as the reference. We measured vector and planar displacements from the reference frame when the feather was aerodynamically loaded with incurrent air moving at 8 ms^{-1}, 12 ms^{-1}, or 16 ms^{-1},

We compared feather anteroposterioral sweep (ϕ) and dorso-ventral bend (ψ) across treatments using affine transformations to root all coordinates in a common "feather-centered" coordinate frame (CCF). Linear translation moved point 2 of the proximal triangle to the origin (0,0,0). The rotation aligned a vector passing through points 2 and 3 of the proximal triangle with the X-axis of the CCF and aligned the

triangle's plane with the CCF X-Y plane. The same transformation was applied to the 8 and 16 ms^{-1} treatments, placing all triangles in the CCF.

The calculation of sweep, bend, and twist were done with vector operations: projections and the cosine formula for dot products. Sweep (ϕ) was defined as the angle between the feather's tip (point 5) projected onto the X-Y plane and the X-axis of the CCF. Bend (ψ) was defined as the angle between the feather tip (point 5) and the X-Y plane of the CCF.

Due to the feathers' relative bend and sweep, two variables associated with twist (θ) were of interest: *Proximodistal twist* (θ_{pd}) is the angle between the proximal triangle's normal vector and the distal triangle's normal vector, with both normals taken at the specified wind speed. Zero degrees would indicate no θ_{pd} and positive angles indicate "nose-down" pitch or *washout* of the distal feather plane in relation to the proximal feather plane under aerodynamic load (Stinton, 2001; Taylor and Thomas, 2002). *Distodistal twist* (θ_{dd}) is the angle between the resting distal triangle's normal vector and the distal triangle's normal vector at a given air speed. This indicates the amount of long-axis twist that occurs distally as velocity increases. Positive angles indicate "nose-down" pitch or washout of the distal triangle under load relative to the distal triangle at rest for a given treatment.

We computed the feather's distal angle of attack under aerodynamic load (α_{dist}) as well as the angle of slip (β). A_{dist} represents the angle between the distal triangle's chord line and the velocity vector in the vertical (pitch) plane. β represents the angle between the velocity vector and the velocity vector in the vertical (pitch) plane.

We observed some differences in the at-rest feather angles between α_{pre}=0° and α_{pre}=13.5° because the feathers were measured over several treatments. These were ±0.9° in bending, ±0.6° in sweep, and ±1.2° in θ_{pd}. We attribute these differences to measurement and digitization error as well as slight movement of the feather barbs between treatments.

Flexural stiffness

We calculated flexural stiffness (EI) using an equation that approximates a uniformly loaded cantilever beam with uniform stiffness (Vogel, 2006):

$$EI = \frac{F\,L^3}{8\,\delta} \qquad \text{(Eq. 4)}$$

Where F is the total resultant force in Newtons, L is the length between point 2 and point 5 in meters, and δ is the deflection of point 5 in meters from its at-rest position to its position under load at 12 ms^{-1} and α_{pre}=13.5°. As calculated here, flexural stiffness is a simplification because lift forces are not necessarily uniformly distributed along the span of the feather. See Worcester (1996) and Wang et al (2012) for a similar measure that uses a point-loaded cantilever beam equation.

Statistical analysis

To test for the statistical significance of effects of α and V upon deflection angles, we used two-way repeated-measures ANOVAs using the afex package in R (R Core Team, 2015; Singmann et al., 2016). We used generalized Eta-squared as a measure of effect size for the ANOVAs. Eta-squared (η^2) can be interpreted as the model having a small effect when η^2=0.02, a medium effect when η^2=0.13, and a large effect when η^2=0.26 (Cohen, 1988). We further compared contrasts between treatments (e.g. 8 ms^{-1} at α_{pre}=13.5° vs 16

ms^{-1} at α_{pre}=13.5°) using post-hoc least-squares means test with Tukey p-value corrections. We examined the potential relationship between deflection and mass using linear models fitted with phylogenetically independent contrasts (PIC, see Felsenstein, 1985). We considered slopes to be significantly different if their 95% confidence intervals did not overlap. We also used a one-way T-test to check for bending-lateral force slopes for differences from zero. The PICs were computed using a majority rules consensus (MRC) tree based on 100 random trees downloaded from birdtree.org (Jetz et al., 2012; Revell, 2012). At-rest angles were calculated twice (at α=0° and 13.5°) to provide a measure of error (see Methods '*Quantifying deflection'*). We log-transformed mass and flexural stiffness data. We report means ± 1 s.d.

RESULTS

Feathers exhibited increased bending, sweep, proximodistal twist, distodistal twist, and slip angles in relation to increased *V* and α_{pre} on average. In contrast, α_{dist} decreased with increased *V* (Fig. 2).

Bending – *V* and α_{pre} both predicted ψ ($p<.001$ for both; Table 1). At α_{pre}=0°, feathers retained their anhedral shape and had negative ψ throughout the range of *V*. In contrast, at 16 ms^{-1}, feathers oriented at α_{pre}=13.5° bent dorsally to 6.4° ± 2.7° on average. At-rest bending angle tended to become more anhedral with mass, ranging from -1.4° ± 0.9° in the merlin to -11.8°±1.1° in the great-horned owl (Fig. 3, Table 2). On average, feathers at rest exhibited a ventral bend resulting in an anhedral angle of -6.4°±3.8°. Thus,

feathers bent dorsally 12.8°±2.3° on average between at-rest angles and peak angles at α_{pre}=13.5° and 16 ms^{-1}.

Sweep – *V* but not α_{pre} predicted ϕ ($p<0.01$ and $p=0.2$, respectively; Table 1). Additionally, the interaction between velocity and α_{pre} had a significant effect on sweep ($p<0.001$). Average ϕ increased with *V*, from 8.3°±3.4° at rest, to 11.6°±2.8° at α_{pre}=0, and 16 ms^{-1} and 11.3°±3.2° at α_{pre}=13.5° and 16 ms^{-1}. All feathers had some degree of at-rest sweep, ranging from 5.0°±0.9° in the red-tailed hawk to 14.5°±0.6° in the great-horned owl.

Proximodistal twist – We found no effect of *V* or α_{pre} on θ_{pd} ($p>0.05$ for both; Table 1). At-rest θ_{pd} was 5.6°±3.5°.

Distodistal twist - *V* but not α_{pre} predicted θ_{dd} ($p=0.05$ and $p=0.3$, respectively; Table 1).

Angle of Attack – α_{dist} decreased with *V* in both α_{pre} treatments ($p<0.01$; Table 1). The starting angle dictated the distal α as well, α_{pre} unsurprisingly influenced α_{dist} as expected ($p<0.001$).

Angle of slip – β significantly increased with *V* but was not affected by α_{pre} ($p<0.001$ and $p=0.7$, respectively). β was also influenced by the interaction between *V* and α_{pre} ($p<0.001$; Table 1).

Deflection and aerodynamic force

Positive changes in ψ were correlated with increased lateral forces (Fig. 4). Force traces of the feathers show lateral force changing in a manner that supports this finding

(Fig. 5). Slopes were significantly non-zero ($p<0.05$, $t=3.6$, T-test). Average lateral forces were 9.5% of the total lift forces at $\alpha_{pre}=13.5°$ at 8 ms^{-1} and 12 ms^{-1} (Table S1).

Flexural stiffness

After accounting for phylogeny, feathers were relatively more flexible with increasing body mass ($EI \propto mass^{1.1\pm0.3}$, $p<0.05$, $R^2=0.67$, 95% CI [0.31 1.89], Fig. 6). This slope did not differ significantly from the measured slope in Worcester (1996) ($mass^{1.29\pm0.29}$) or predicted slope based on geometric similarity ($mass^{1.67}$).

DISCUSSION

Our experiment revealed that feathers bend, twist, and sweep in a complex three-dimensional manner that reoriented aerodynamic force. The feathers deflected passively in response to changes in V and α_{pre}, and deflection varied among species. The underlying shape and structure that influences deflection may therefore be adapted to unique species-specific aeroecological drivers of selection (e.g. Lockwood et al., 1998). This experiment is the first to quantify three-dimensional deflection of feathers in response to aerodynamic forces, and provides novel insight into the functional significance of feather deflection during steady translation that emulates gliding flight.

Bird feathers interact with air flow in a manner that is more complex than rigid airfoils. Feathers deflect passively in response to aerodynamic forces without input from the bird (e.g. Carruthers et al., 2007). In contrast, traditional aircraft are generally built with the stiffest wings possible to prevent passive deflection. Instead, pilots manipulate morphing by adjusting inflexible control surfaces that redirect airflow (Stinton, 2001).

However, recent experimentation with passive morphing wings in MAVs have yielded interesting results (Shyy et al., 2010). For example, a study exploring passive morphing ornithopter wings used compliant spines inserted into the wings' leading edge to increase lift by 16% and reduce power consumption by 45% (Wissa et al., 2011). Our findings illustrate that bird feathers exhibit significant deflection in response to both changes in V and α, and that this morphing increases the effective range of α for feathers compared with a rigid airfoil.

Passive aeroelastic deflection of feathers may reduce the need for dynamic control input (Thomas and Taylor, 2001; Taylor and Thomas, 2002; Carruthers et al., 2007). Birds often fly in turbulent aerial habitat, and our results showed that feathers deflected to accommodate changes in airflow direction and velocity. Thus, passive response to aerodynamic perturbations may reduce the need for corrective sensorimotor input. Employing biomimetic design principles that are inspired by feather flexibility could improve passive aerodynamic function of manufactured airfoils by increasing stability and reducing the need for active control.

Effects of deflection

Bending reoriented lift such that some of the resultant force was directed laterally towards the proximal end of the feather (Fig. 4). The bent feathers worked much like the dihedral and anhedral wings of aircraft (Sachs and Holzapfel, 2007). Dihedral angles are known to increase passive lateral (also termed roll or spiral mode) stability in aircraft by orienting the lift forces over the center of mass and inducing sideslip (Thomas and Taylor, 2001). Negative, anhedral bending, such as seen in the great-horned owl and osprey at low

velocity, is known to contribute to instability and enhance maneuverability (Thomas and Taylor, 2001).

While the selective drivers of feather bending in falcons, hawks, and owls remain unknown, we hypothesize that they may be due to aeroecological factors associated with differences in flight. Hawks and falcons are known for flying in turbulent, thermic conditions during the day. These flights can be violently unstable due to convective updrafts, wind shear, and surface winds (Reynolds et al., 2014). Thus, it may be that these birds have feathers with more dihedral bend to provide lateral stability. Conversely, owls fly at night in forested habitat where turbulence is minimal. In these species, we might expect feathers to exhibit more anhedral bend so that maneuverability is increased, as selection on stability is relaxed. Osprey, which also had anhedrally bent feathers, fly over water where turbulence is minimal. Cumulatively, our findings hint that differences in feather deflection may be due to differences in flight conditions. In contrast, these differences may be phylogenetic in nature. Future comparative research with a larger sample size could test these hypotheses.

Sweep varied significantly as a function of V but not α_{pre} (Fig. 2, Table 1). This indicates that profile drag was a more significant factor than lift because feathers at α=13.5° had higher lift but exhibited similar sweep angles (Fig. 3). In the present study it appears that sweep was a product of profile drag pushing the feather caudally. Sweep causes some portion of the bending moment to be converted into axial torsion, thus distributing the aerodynamic load across all moments (Stinton, 2001). It is therefore possible that sweep may work to prevent breakage via bending forces at high speed or high α, although more testing will be needed to verify this hypothesis.

There was no clear relationship between α_{pre}, *V*, and proximodistal twist. Proximodistal twist both increased and decreased among different species. These results suggest two possible phenomena: 1) twist was occurring at both the proximal and distal planes in ways that make interpretation difficult, or 2) twist changed in a non-linear fashion with α and *V*. Long-axis twist occurred along the entire length of the feathers' rachises and calamuses. Generally, this resulted in proximal attack angles that increased with velocity, particularly when α_{pre}=13.5°. Thus, since both proximal and distal attack angles were changing concomitantly, variation was effectively doubled. It is also possible that experimental error contributed to this because small errors in the digitization of the points or differences in the actual feathers between treatments could have led to deviations in the angles measured.

Distodistal twist increased with *V* but not α. In addition to the mean values, the range of distodistal twist values also increased with velocity (Fig. 2) which is particularly influenced by the flexible feathers of the American kestrel and Cooper's hawk (Fig. 3). Distodistal twist provided a measure of twistiness at the feather tip and all feathers twisted in a pitch-down motion as velocity increased.

Distal angle of attack (α_{dist}) significantly decreased with increasing *V*, which is corroborated by the increased distodistal twist (Fig. 2). This reduction in α due to twisting deflection has direct consequences on lift and drag. As the local distal α decreased with increasing velocity, lift and drag forces were also reduced (Fig. 5). Additionally, force coefficients did not increase with α as much as the airfoil (Fig 5). The feathers continued to produce increasing amounts of lift as they rotated through α_{pre}=27° while the airfoil

stalled at α_{pre}=22.5° at 8 ms^{-1} and at α_{pre}=13.5° at 12 ms^{-1}. This indicates that feather deflection likely delayed the onset of stall.

Aerodynamic forces

The force data show two trends: 1) feathers produced lateral forces that altered stability, and 2) feathers exhibited delayed stall compared to a rigid airfoil (Fig. 5). The presence of lateral force confirms that feather deflection (principally bending) reoriented aerodynamic force medially. Thus, bending primary feathers confer lateral stability in flight (Thomas and Taylor, 2001). Moreover, this suggests that future wind tunnel research of living and emulated bird flight should account for forces along all three axes—not just lift or drag. While primary feathers represent a small percentage (8.6% ± 2.2% on average) of the total wing surface area, their function at the wing tip is especially important for two reasons: 1) during flapping flight, these feathers are producing higher aerodynamic forces because they are moving faster (Usherwood and Ellington, 2002b; Usherwood et al., 2003; Klaassen van Oorschot et al., 2016), and 2) these feathers are the furthest from the center of mass, thus providing the greatest torque moment during roll and yaw maneuvers (Thomas and Taylor, 2001; Sachs and Moelyadi, 2006; Sachs and Holzapfel, 2007).

Flexural stiffness

We found that feathers were more flexible than expected according to scaling models of geometric or elastic similarity. However, the large variance we observed precludes any definitive conclusions about the true scaling relationship of feather stiffness

and mass. We attribute this variance to our small sample size, and future studies could include a larger comparative dataset to address this issue. Our findings are consistent with Worcester (1996) and Wang et al. (2012), but if our mean slope is correct, feathers become even more flexible as birds get heavier than previously thought. We anticipate differences in stiffness are likely tied to ecological and behavioral factors such as flight speed and foraging style, and our experiment just examines flexural stiffness in a small subset of raptors. Thus, caution should be taken when interpreting our results. Our measure of flexural stiffness under aerodynamic load is likely more relevant to the bird during flight, however. The large deflections observed in this experiment warrant further examination in a comparative context.

CONCLUSIONS

Our results showed that feathers passively deflected in response to changes in V and α. Feather deflection increased lateral force and delayed stall in comparison to a rigid airfoil. In addition to dynamic morphing of wings (e.g. Klaassen van Oorschot et al., 2016), passive deflection of individual feathers provides yet another layer of complexity to avian aerodynamics. Generally, studies of biological airfoils have reported force measurements in two axes: lift and drag. Our results indicate that future studies of flexible airfoils should consider the three-dimensionality of aerodynamic forces. Moreover, our findings suggest that feather flexibility may be beneficial in terms of stability and stall avoidance. The utility of understanding passive deflection in bird feathers is particularly relevant to manufactured morphing airfoils, especially given recent developments in flexible materials and additive manufacturing (Barbarino et al., 2011; Sun et al., 2016).

ACKNOWLEDGEMENTS

We thank Ho Kwan Tang, Paige Folsom, Ondi Crino, and Kileen Marshall for their help and support.

FUNDING

This research was supported by National Science Foundation grants GRFP DGE−1313190 to BKVO and IOS-0923606, IOS-0919799 and CMMI 1234747 to BWT.

REFERENCES

Bachmann T, Emmerlich J, Baumgartner W, Schneider JM, Wagner H. 2012. Flexural stiffness of feather shafts: geometry rules over material properties. J Exp Biol 215:405–415.

Bachmann T, Klän S, Baumgartner W, Klaas M, Schröder W, Wagner H. 2007. Morphometric characterisation of wing feathers of the barn owl Tyto alba pratincola and the pigeon Columba livia. Front Zool 4:23.

Barbarino S, Bilgen O, Ajaj RM, Friswell MI, Inman DJ. 2011. A Review of Morphing Aircraft. J Intell Mater Syst Struct 22:823–877.

Brown RHJ. 1963. The flight of birds. Biol Rev 38:460–489.

Carruthers AC, Thomas ALR, Taylor GK. 2007. Automatic aeroelastic devices in the wings of a steppe eagle (Aquila nipalensis). J Exp Biol 210:4136–4149.

Cohen J. 1988. Statistical power analysis for the behavioral sciences. 2nd ed. Hillsdale, NJ: Erlbaum.

Corning WR, Biewener AA. 1998. In vivo strains in pigeon flight feather shafts: implications for structural design. J Exp Biol 201:3057–3065.

Erlich PR, Dobkin DS, Wheye D. 1988. The birder's handbook: A field guide to the natural history of North American birds. New York: Simon & Schuster.

Felsenstein J. 1985. Phylogenies and the Comparative Method. Am Nat 125:1–15.

Fluck M, Crawford C. 2014. A lifting line model to investigate the influence of tip feathers on wing performance. Bioinspir Biomim 9:46017.

Graham RR. 1932. Safety devices in wings of birds. Aeronaut J 36:24–58.

Hedrick TL. 2008. Software techniques for two- and three-dimensional kinematic measurements of biological and biomimetic systems. Bioinspir Biomim 3:34001.

Heo H, Ju J, Kim D-M, Jeon C-S. 2011. Passive morphing airfoil with honeycombs. ASME 2011 Int Mech Eng Congr Expo 64350:263–271.

Jetz W, Thomas GH, Joy JB, Hartmann K, Mooers AO. 2012. The global diversity of birds in space and time. Nature 491:444–448.

Klaassen van Oorschot B, Mistick EA, Tobalske BW. 2016. Aerodynamic consequences of wing morphing during emulated take-off and gliding in birds. J Exp Biol 219:3146–3154.

Klaassen van Oorschot B, Tang HK, Tobalske BW. 2017. Phylogenetics and ecomorphology of emarginate primary feathers. J Morphol in press.

KleinHeerenbrink M, Warfvinge K, Hedenström A. 2016. Wake analysis of aerodynamic components for the glide envelope of a jackdaw (Corvus monedula). J Exp Biol 219:1572–1581.

Lindhe Norberg UM. 2002. Structure, form, and function of flight in engineering and the living world. J Morphol 252:52–81.

Lingham-Soliar T. 2014. Feather structure, biomechanics and biomimetics: The incredible lightness of being. J Ornithol 155:323–336.

Lockwood R, Swaddle JP, Rayner JMV. 1998. Avian wingtip shape reconsidered: wingtip shape indices and morphological adaptations to migration. J Avian Biol 29:273–292.

Norberg RÅ. 1985. Function of vane asymmetry and shaft curvature in bird flight feathers; inferences on flight ability of Archaeopteryx. In: Ostrom JH,, Hecht MK,, Viohl G,, Wellnhofer P, editors. The beginnings of birds Eichstatt: Jura Museum. p. 303–318.

Pankonien AM, Inman DJ. 2014. Aeroelastic performance evaluation of a flexure box morphing airfoil concept. Proc SPIE 9057 9057:905716.

Pap PL, Osváth G, Sándor K, Vincze O, Bărbos L, Marton A, Nudds RL, Vágási CI. 2015. Interspecific variation in the structural properties of flight feathers in birds indicates adaptation to flight requirements and habitat. Funct Ecol n/a-n/a.

Pennycuick CJ, Lock A. 1976. Elastic energy storage in primary feather shafts. J Exp Biol 64:677–689.

Purslow PP, Vincent JFV. 1978. Mechanical Properties of primary feathers from the pigeon. J Exp Biol 72:251–260.

R Core Team. 2015. R: A language and environment for statistical computing.

Rayner JMV. 1988. Form and Function in Avian Flight. Curr Ornithol 5:1–66.

Revell LJ. 2012. phytools: an R package for phylogenetic comparative biology (and other things). Methods Ecol Evol 3:217–223.

Reynolds K V., Thomas ALR, Taylor GK. 2014. Wing tucks are a response to atmospheric turbulence in the soaring flight of the steppe eagle *Aquila nipalensis*. J R Soc Interface 11:20140645.

Sachs G, Holzapfel F. 2007. Flight Mechanic and Aerodynamic Aspects of Extremely Large Dihedral in Birds. In: 45th AIAA Aerospace Sciences Meeting and Exhibit Reston, Virigina: American Institute of Aeronautics and Astronautics. p. 1–12.

Sachs G, Moelyadi MA. 2006. Effect of slotted wing tips on yawing moment characteristics. J Theor Biol 239:93–100.

Shyy W, Aono H, Chimakurthi SK, Trizila P, Kang CK, Cesnik CES, Liu H. 2010. Recent progress in flapping wing aerodynamics and aeroelasticity. Prog Aerosp Sci 46:284–327.

Singmann H, Bolker B, Westfall J, Aust F. 2016. afex: Analysis of Factorial Experiments.

Sofla AYN, Meguid SA, Tan KT, Yeo WK. 2010. Shape morphing of aircraft wing: Status and challenges. Mater Des 31:1284–1292.

Stinton D. 2001. The Design of the Airplane, Second Edition. Washington, DC: American Institute of Aeronautics and Astronautics, Inc.

Sun J, Guan Q, Liu Y, Leng J. 2016. Morphing aircraft based on smart materials and structures: A state-of-the-art review. J Intell Mater Syst Struct 27:1045389X16629569-.

Swaddle JP, Lockwood R. 2003. Wingtip shape and flight performance in the European starling Sturnus vulgaris. Ibis 145:457–464.

Taylor GK, Thomas ALR. 2002. Animal flight dynamics II. Longitudinal stability in flapping flight. J Theor Biol 214:351–370.

Thomas ALR, Taylor GK. 2001. Animal flight dynamics I. Stability in gliding flight. J Theor Biol 212:399–424.

Tobalske BW, Puccinelli LA, Sheridan DC. 2005. Contractile activity of the pectoralis in the zebra finch according to mode and velocity of flap-bounding flight. J Exp Biol 208:2895–2901.

Trowbridge CC. 1906. Interlocking of emarginate primary feathers in flight. Am J Sci 21:145–169.

Tubaro PL. 2016. A comparative study of aerodynamic function and flexural stiffness of outer tail feathers in birds. J Avian Biol 34:243–250.

Tucker VA. 1993. Gliding birds: reduction of induced drag by wing tip slots between the primary feathers. J Exp Biol 180:285–310.

Tucker VA. 1995. Drag reduction by wing tip slots in a gliding Harris' hawk, Parabuteo unicinctus. J Exp Biol 198:775–781.

Usherwood JR, Ellington CP. 2002a. The aerodynamics of revolving wings I. Model hawkmoth wings. J Exp Biol 205:1547–1564.

Usherwood JR, Ellington CP. 2002b. Aerodynamics of Revolving Wings. 204:1565–1576.

Usherwood JR, Hedrick TL, Biewener AA. 2003. The aerodynamics of avian take-off from direct pressure measurements in Canada geese (Branta canadensis). J Exp Biol 206:4051–4056.

Vogel S. 2006. Comparative Biomechanics. 580.

Wang X, Nudds RL, Palmer C, Dyke GJ. 2012. Size scaling and stiffness of avian primary feathers: Implications for the flight of Mesozoic birds. J Evol Biol 25:547–555.

Wissa A, Tummala Y, Jr JEH, Frecker M, Brown A, Hubbard Jr. JE, Frecker M, Brown A. 2011. Testing of Novel Compliant Spines for Passive Wing Morphing. Smasis 1–10.

Withers PC. 1981. The aerodynamic performance of the wing in red-shouldered hawk (Buteo linearis) and a possible aeroelastic role of wing-tip slots. Ibis 123:239–247.

Worcester SE. 1996. The scaling of the size and stiffness of primary flight feathers. J Zool 239:609–624.

TABLES

Table 1. Summary of repeated-measures ANOVA for deformation of feathers at different airspeeds (V) and starting attack angles (α_{pre}).

Deformation type	Model terms	D.F.	F-statistic	Generalized ETA-squared	P-value
Bend (ψ)	V	1.45, 8.70	53.8	.41	**<0.001**
	α_{pre}	1, 6	46.2	.41	**<0.001**
	V * α_{pre}	1.31, 7.84	49.6	.21	**<0.001**
Sweep (ϕ)	V	1.14, 6.84	17.6	.131	**<0.01**
	α_{pre}	1, 6	1.8	.007	0.2
	V * α_{pre}	1.82, 10.91	20.1	.01	**<0.001**
PD Twist (θ_{pd})	V	1.65, 9.92	0.95	.06	0.4
	α_{pre}	1, 6	2.01	.02	0.2
	V * α_{pre}	1.41, 8.47	0.07	.003	0.9
DD Twist (θ_{dd})	V	2.12, 12.73	3.9	.16	**0.05**
	α_{pre}	1, 6	1.57	.06	0.3
	V * α_{pre}	1.99, 11.93	0.92	.02	0.4
AoA (α_{post})	V	1.92, 11.5	10.5	.22	**<.01**
	α_{pre}	1, 6	6.83	.61	**<0.001**
	V * α_{pre}	1.93, 11.56	10.5	.04	0.2
AoS (β)	V	1.09, 6.53	34.6	0.25	**<0.001**
	α_{pre}	1, 6	0.17	0.001	0.7
	V * α_{pre}	2.51, 15.09	9.40	0.01	**<.001**

Table 2. Deflection angles for individuals at each V and α

Species	Velocity	α_{pre}	Bend (ψ)	Sweep (ϕ)	PD Twist (θ_{pd})	DD Twist (θ_{dd})	AOA (α_{dist})	AOS (β)
AMKE	0	0	-4.5	6.7	8.5	0	9.7	10.7
	8	0	-2.8	8	6.4	1.8	2.1	20.7
	12	0	-2	10.4	3.4	3.5	4.3	21.8
	16	0	-3.2	13.1	0.5	7.1	12.9	11.5
	0	13.5	-2.5	7.5	8.9	0	-1.1	9
	8	13.5	3.5	8.2	6.3	1	7.6	13.7
	12	13.5	6.1	9	5.9	12.9	-2.4	2.1
	16	13.5	8	11.5	8.3	14.2	7.2	13.4
MERL	0	0	-2.3	6.2	12.1	0	7.4	21.1
	8	0	-0.8	7.6	5.6	3.5	-4.3	11.6
	12	0	0.7	8.9	9.7	0	0.2	19.6
	16	0	2.3	11.3	4.1	3.5	-2.7	15.8
	0	13.5	-0.5	6.3	8.4	0	23.6	9.4
	8	13.5	1.8	7.6	8	0.9	7.5	19.2
	12	13.5	4.7	8.6	8.7	0.6	18.9	16.8
	16	13.5	8.5	9.3	5.2	0.2	22.4	9.5
COHA	0	0	-3.8	10	0.3	0	1.2	23.2
	8	0	-1.2	11.3	0.5	1.5	2.9	22.5
	12	0	0.4	12.4	0.3	3.9	8.9	14.1
	16	0	0.1	13.4	5.5	1.7	-0.9	9.6
	0	13.5	-5.7	12.2	9.8	0	7.5	15.3
	8	13.5	0.2	13.6	7.2	18.7	2.4	4.9
	12	13.5	6.3	14.1	0	13.1	5.3	18.8
	16	13.5	9.3	14.7	0.9	14.3	2.3	24.9
RTHA	0	0	-9.6	4.1	3.8	0	12	11.2
	8	0	-5.4	5.5	0.8	5.4	5.2	22.7
	12	0	-4.9	7	0.8	4.4	9.4	30.9
	16	0	-6.7	10.2	6	1	9	23.5
	0	13.5	-9.2	5.8	3.4	0	19.2	18.7
	8	13.5	3	7	1.5	6	5.8	10.4
	12	13.5	8.4	7.6	1.2	4.2	14	23.7
	16	13.5	7.6	10.7	7.1	0	6.5	17.9
PEFA	0	0	-3.8	7.5	6.3	0	19.4	16.6
	8	0	-3.2	8.4	5.4	0.3	15.5	8
	12	0	-2.3	9.3	4.4	1.1	7.2	17.1
	16	0	-1.3	10.5	1.2	6.1	11	28.4
	0	13.5	-4.2	9.3	6.5	0	12.4	22
	8	13.5	-1.3	10.2	4.4	1.2	21.5	17.7
	12	13.5	2.5	11.1	7.4	2.4	9.4	8.9
	16	13.5	6.2	11.8	1.9	1.9	20.9	20.3
GHOW	0	0	-12.8	13.9	3.2	0	3.1	23.8
	8	0	-11	14.2	2.5	0.4	11.6	16.8
	12	0	-9.8	14.9	2	1.7	-2.2	10.6
	16	0	-10.2	15.7	6.4	0.6	5.6	17.3
	0	13.5	-10.7	15.1	1.2	0	0.9	8
	8	13.5	-5.7	15.1	4.1	2.1	2.7	23.7
	12	13.5	1	14.4	0	1.8	-3.4	27.1
	16	13.5	2.4	15.1	3.2	1	1.2	25.1
OSPR	0	0	-10.4	5.3	3.4	0	12.3	4.4
	8	0	-9.3	5.8	3	0.7	22	13.5
	12	0	-8.9	6.3	3.6	0.3	11.2	-0.5
	16	0	-9.6	6.9	6	2.7	20.3	13.9
	0	13.5	-9.3	6	2.8	0	22.1	24.7
	8	13.5	-4.3	5.9	1.6	2	13.7	19.4
	12	13.5	0.8	5.7	5	0.4	22.9	12.6
	16	13.5	3	5.9	9.5	3.5	13.3	6.6

FIGURES

Figures 1a and 1b: Diagram of feather, proximal triangle and frame (points {1,2,3}, proximal green frame), distal triangle and frame (points {4,5,6}, distal green frame), CCF frame ({$\hat{X}$, $\hat{Y}$, $\hat{Z}$}), air flow (v), sweep (φ), and bend (ψ).

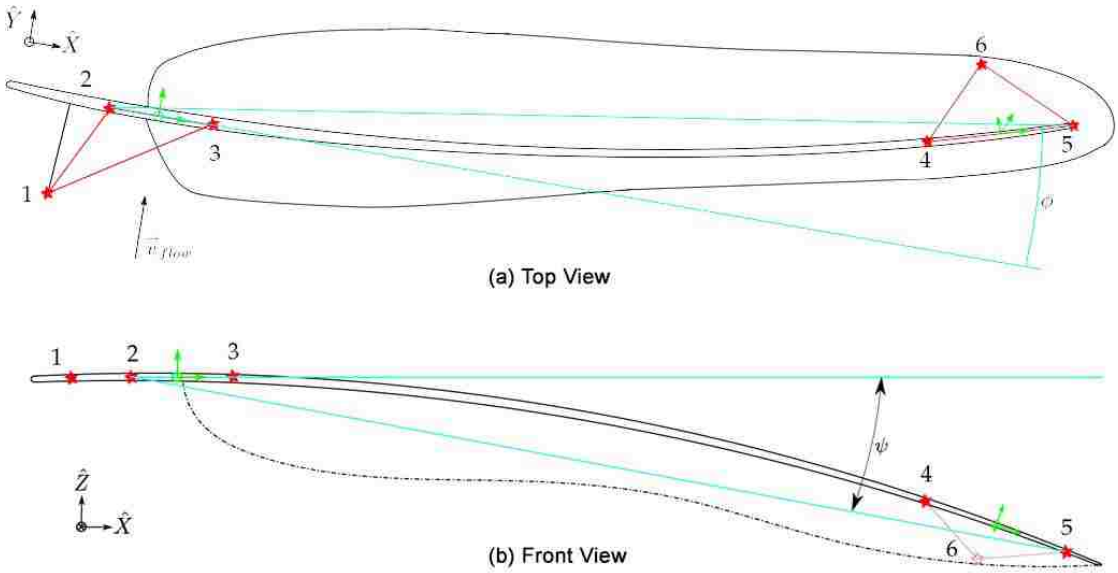

Figure 2: Boxplots of deflection averages at 0 ms^{-1}, 8 ms^{-1}, 12 ms^{-1}, 16 ms^{-1} and α_{pre}=0° and 13.5°. Minimum, first quartile, median, third quartile, and maximum shown.

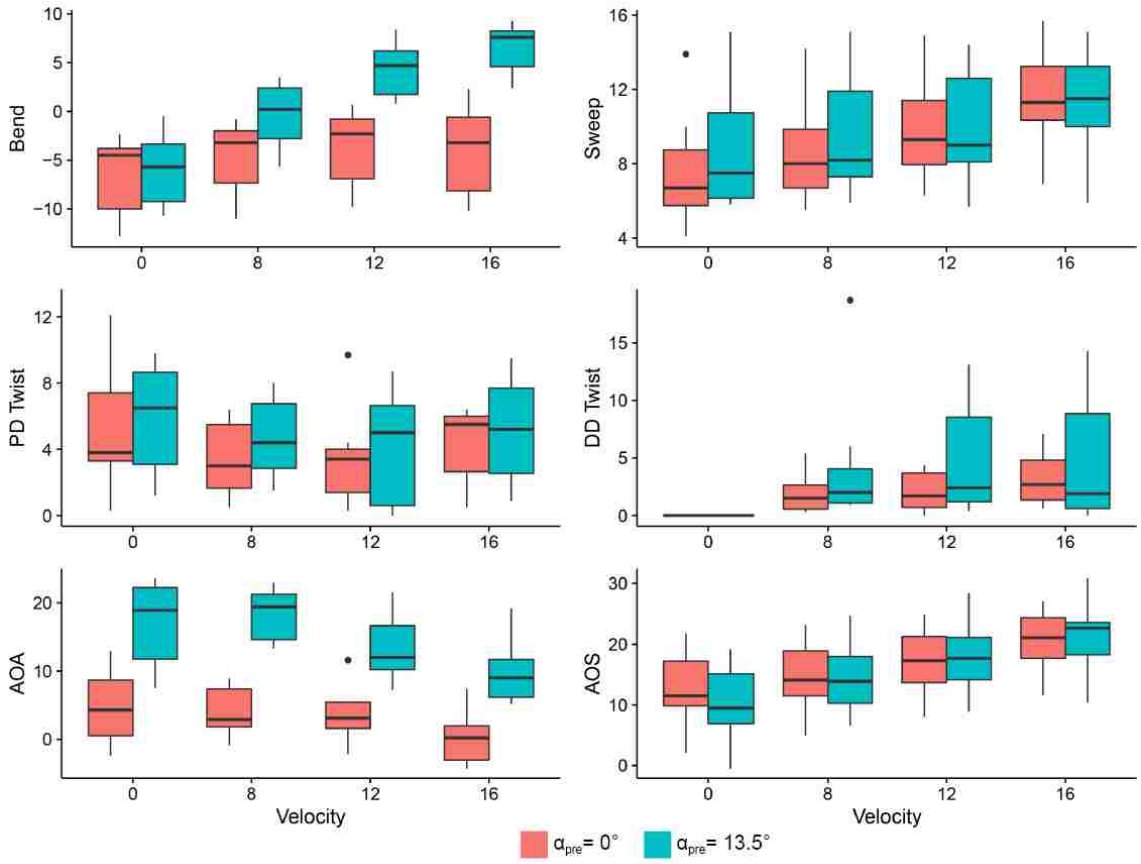

Figure 3: Individual deflection angles by species, α_{pre} (circles represent 0° and diamonds represent 13.5°), and velocity (represented by color).

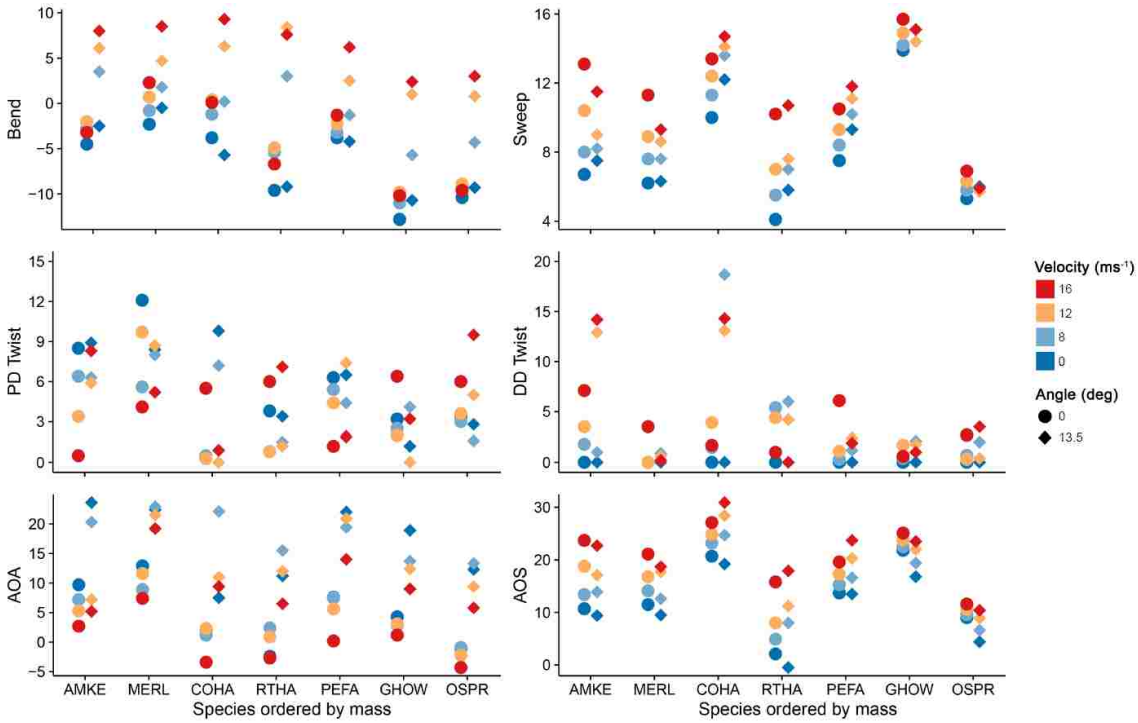

Figure 4: Proximal lateral force increases as feathers bend ventrally with increasing air velocity.

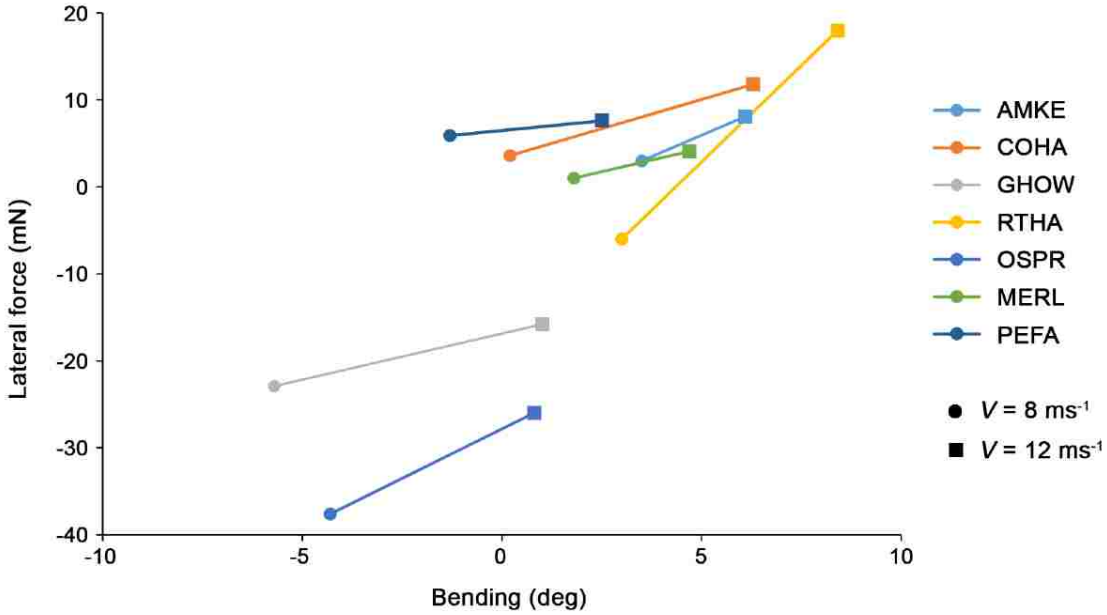

Figure 5: Coefficients of vertical (C_V), horizontal (C_H), and lateral force (C_K) according to velocity and attack angle. Note that among all samples, only the airfoil exhibited stall.

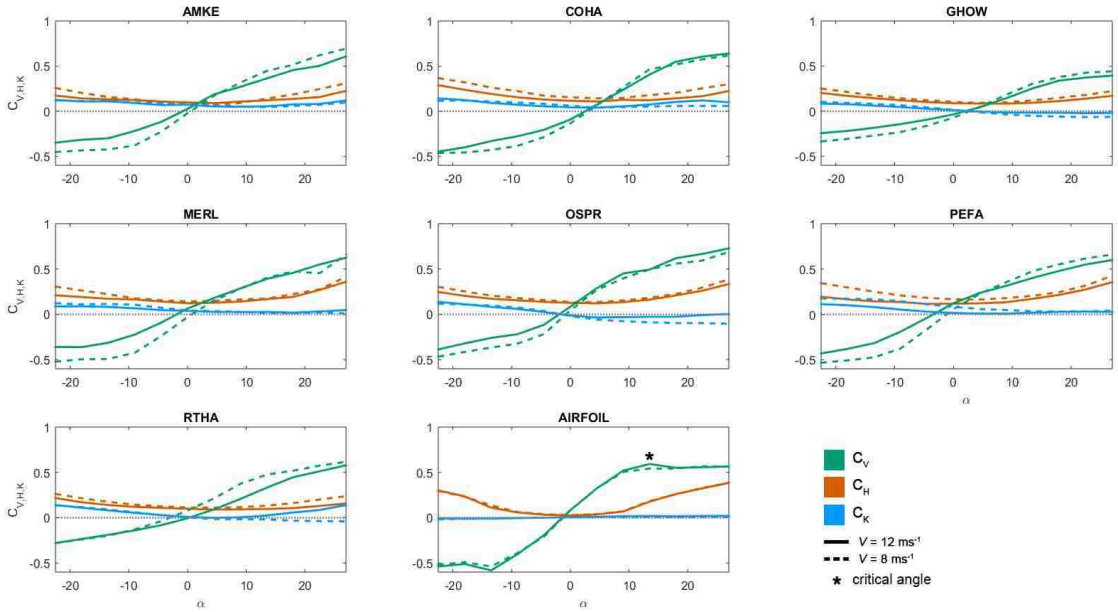

Figure 6: Linear model of phylogenetically independent contrasts for log-transformed flexural stiffness and body mass.